Multiple emplacement and exhumation history of the Late Mesozoic Dayunshan-Mufushan batholith in Southeast China and its tectonic significance: 1. Structural analysis and geochronological constraints

Wenbin Ji, Michel Faure, Wei Lin, Yan Chen, Yang Chu, Zhenhua Xue

AGU PUBLICATIONS

JGR

Journal of Geophysical Research: Solid Earth

RESEARCH ARTICLE
10.1002/2017JB014597

This article is a companion to Ji et al. (2017), https://doi.org/10.1002/2017JB014598.

Key Points:
- The Dayunshan–Mufushan batholith recorded a multiple emplacement and exhumation history
- An integrated multidisciplinary investigation improves our understanding on the Late Mesozoic tectonomagmatism in southeast China
- Two deformation events in relation to batholith emplacement and subsequent exhumation are identified

Supporting Information:
- Table S1

Correspondence to:
W. Lin,
linwei@mail.iggcas.ac.cn

Citation:
Ji, W., Faure, M., Lin, W., Chen, Y., Chu, Y., & Xue, Z. (2018). Multiple emplacement and exhumation history of the Late Mesozoic Dayunshan–Mufushan batholith in southeast China and its tectonic significance: 1. Structural analysis and geochronological constraints. *Journal of Geophysical Research: Solid Earth*, *123*. https://doi.org/10.1002/2017JB014597

Received 25 JUN 2017
Accepted 30 NOV 2017
Accepted article online 7 DEC 2017

Multiple Emplacement and Exhumation History of the Late Mesozoic Dayunshan–Mufushan Batholith in Southeast China and Its Tectonic Significance: 1. Structural Analysis and Geochronological Constraints

Wenbin Ji[1,2], Michel Faure[2], Wei Lin[1], Yan Chen[2], Yang Chu[1], and Zhenhua Xue[1,2]

[1]State Key Laboratory of Lithospheric Evolution, Institute of Geology and Geophysics, Chinese Academy of Sciences, Beijing, China, [2]Institut des Sciences de la Terre d'Orléans, UMR 7327, Université d'Orléans, Orléans, France

Abstract The South China Block (SCB) experienced a polyphase reworking by the Phanerozoic tectonothermal events. To better understand its Late Mesozoic tectonics, an integrated multidisciplinary investigation has been conducted on the Dayunshan–Mufushan composite batholith in the north-central SCB. This batholith consists of two major intrusions that recorded distinct emplacement features. According to our structural analysis, two deformation events in relation to batholith emplacement and subsequent exhumation are identified. The early one (D_1) was observed mostly at the southern border of the batholith, characterized by a top-to-the-SW ductile shearing in the early-stage intrusion and along its contact zone. This deformation, chiefly associated with the pluton emplacement at ca. 150 Ma, was probably assisted by farfield compression from the northern Yangtze foreland belt. The second but main event (D_2) involved two phases: (1) ductile shearing (D_{2a}) prominently expressed along the Dayunshan detachment fault at the western border of the batholith where the syntectonic late-stage intrusion and minor metasedimentary basement in the footwall suffered mylonitization with top-to-the-NW kinematics; and (2) subsequent brittle faulting (D_{2b}) further exhumed the entire batholith that behaved as rift shoulder with half-graben basins developed on its both sides. Geochronological constraints show that the crustal ductile extension occurred during 132–95 Ma. Such a Cretaceous NW–SE extensional tectonic regime, as indicated by the D_2 event, has been recognized in a vast area of East Asia. This tectonism was responsible not only for the destruction of the North China craton but also for the formation of the so-called "southeast China basin and range tectonics."

1. Introduction

One notable tectonic phenomenon in East Asia during the Late Mesozoic is the destruction of the North China craton (NCC), characterized by lithospheric thinning (at least 100 km removal) and transformation of the lithospheric mantle properties (e.g., Menzies et al., 2007; Wu et al., 2008; R. X. Zhu et al., 2012). Extensional tectonics has been attested to be one of the crustal-scale responses to cratonic destruction. Late Mesozoic rift basins and extensional domes, especially metamorphic core complexes (MCCs), are widely developed in the NCC and its adjacent regions, indicating a large-scale continental extension (e.g., Charles et al., 2011, 2012, 2013; Davis & Darby, 2010; Davis et al., 2002; Ji, Lin, Faure, Shi, et al., 2017; Lin, Charles, et al., 2013; Lin, Faure, et al., 2008, 2013; Lin & Wang, 2006; Lin et al., 2011, 2015; Liu et al., 2005, 2013; Meng, 2003; Wang et al., 2011, 2012; G. Zhu et al., 2012, 2015). Coeval with the NCC destruction, the South China Block (SCB) also seems to experience continental extension. The Late Mesozoic geology of the eastern SCB is featured by widespread magmatism and numerous small rift basins, forming the so-called "southeast China basin and range tectonics" (Gilder et al., 1991, 1996; Li, 2000; J. H. Li et al., 2014; Shu et al., 2009; D. Z. Wang & Shu, 2012; Zhou & Li, 2000; Zhou et al., 2006). Despite intensive studies over the past decades focused on the cratonic destruction, the temporal–spatial configuration and geodynamic mechanisms of the Late Mesozoic extensional tectonics in the eastern China is still enigmatic (see Lin, Charles, et al., 2013, for a discussion).

When compared with North China, as well as with the western United States, typical MCC as the locus of intense tectonic exhumation of deep crustal rocks is rarely developed in South China. As depicted in Figure 1, so far only a few extensional massifs (mainly magmatic domes or syntectonic plutons bounded by ductile normal faults) have been documented in hinterland of the SCB, such as the Wugongshan (Faure et al., 1996), Lushan (Lin et al., 2000; Q. B. Zhu, Yang, & Wang, 2010), Hongzhen (G. Zhu et al., 2010),

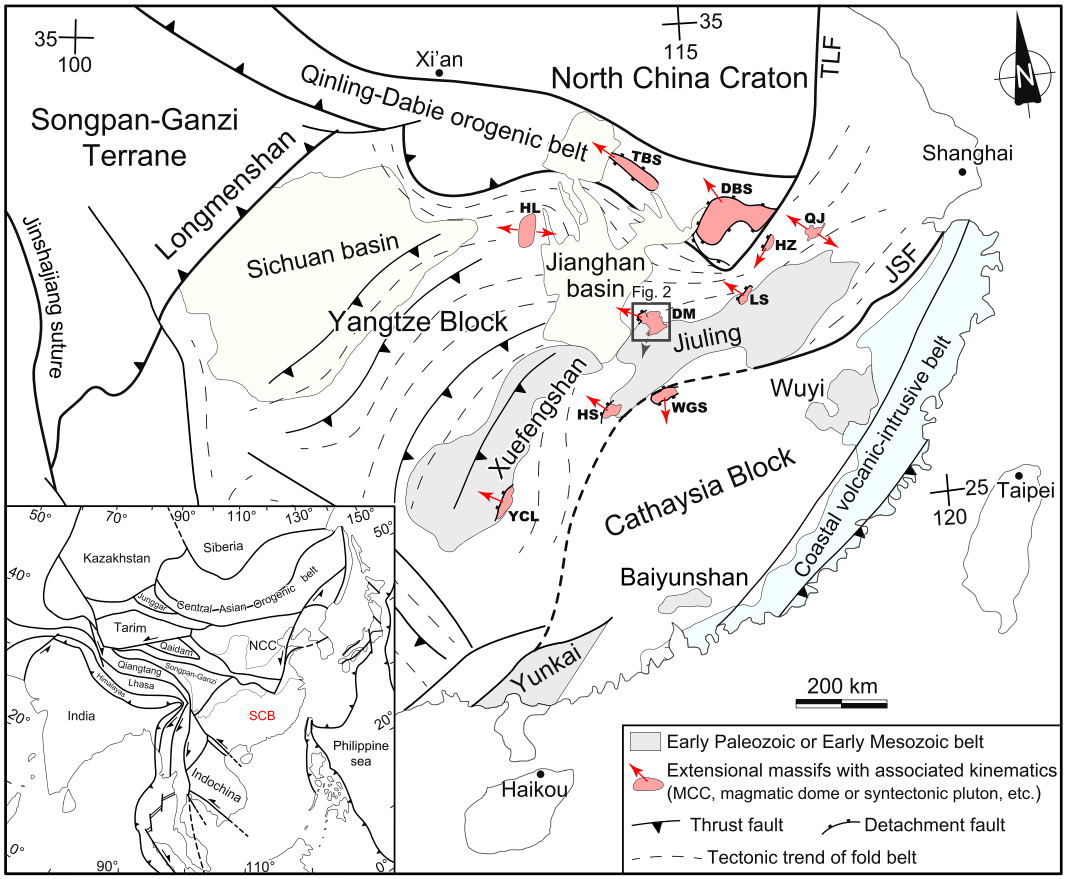

Figure 1. Tectonic sketch of the SCB and location of the Dayunshan–Mufushan batholith. NCC, North China craton; SCB, South China Block; TLF, Tan-Lu fault; JSF, Jiangshan-Shaoxing fault, representing the Neoproterozoic suture zone between the Yangtze and Cathaysia blocks. Several Late Mesozoic extensional massifs in South China: TBS, Tongbaishan antiform (Lin et al., 2015); DBS, Dabieshan MCC (Ji, Lin, Faure, Shi, et al., 2017; Lin et al., 2015); HL, Huangling dome (Ji et al., 2014); QJ, Qingyang–Jiuhua batholith (Wei, Chen, et al., 2014; Wei, Martelet, et al., 2014); HZ, Hongzhen dome (G. Zhu et al., 2010); LS, Lushan dome (Lin et al., 2000; Q. B. Zhu, Yang, & Wang, 2010); WGS, Wugongshan dome (Faure et al., 1996); DM, Dayunshan–Mufushan batholith (this study); HS, Hengshan dome (Li, Zhang, Dong, Su, et al., 2013; Li et al., 2016; Wei et al., 2016); YCL, Yuechengling dome (our unpublished data).

Hengshan (Li, Zhang, Dong, Su, et al., 2013; Li et al., 2016; Wei et al., 2016), and Huangling (Ji et al., 2014). Although these case studies provide significant information on the Late Mesozoic extensional tectonics in South China, some critical issues are still not settled: (1) structural style, especially kinematics of the continental extension; and (2) onset and duration of the extensional tectonic regime. It is noteworthy that Late Mesozoic compressional tectonics has also been recognized in South China. For instance, Yan et al. (2009, 2003) suggested that the pre-Late Cretaceous thin-skinned tectonic system extending from the Xuefengshan belt to the Sichuan basin was produced by westward progressive collision between the North and South China blocks. To the north of the Sichuan basin, the Dabashan orocline of the South Qinling orogen experienced NE–SW intracontinental shortening during the Middle Jurassic to Early Cretaceous (Hu et al., 2012; Li, Zhang, Dong, & Shi, 2013; Shi et al., 2012). In the coastal region, a regional NW-directed backthrusting that developed along the Changle–Nan'ao belt has been interpreted as a response to the Early Cretaceous collision of the West Philippines microcontinent with the SCB (Wei et al., 2015). These extensional and compressional events distinguished in different parts of the SCB lead to the difficulty in understanding the Mesozoic geodynamics of South China (Li et al., 2012; J. H. Li et al., 2014).

The Dayunshan–Mufushan batholith is located in the middle segment of the NE–SW trending Xuefengshan–Jiuling belt of the central SCB (Figures 1 and 2). It is a composite batholith with Late Jurassic to Early Cretaceous granitic intrusions (Ji, Lin, Faure, Chen, et al., 2017; L. X. Wang et al., 2014). Li and Yu (1991) firstly brought in a MCC model for the ore-controlling structures of Pb–Zn mineralization related to emplacement of this batholith. Further, Yu, Ye, and Peng (1998) confirmed that the Dayunshan massif (i.e., the western tongue-shaped part of the batholith) has structural features of a typical MCC: the core is occupied by a

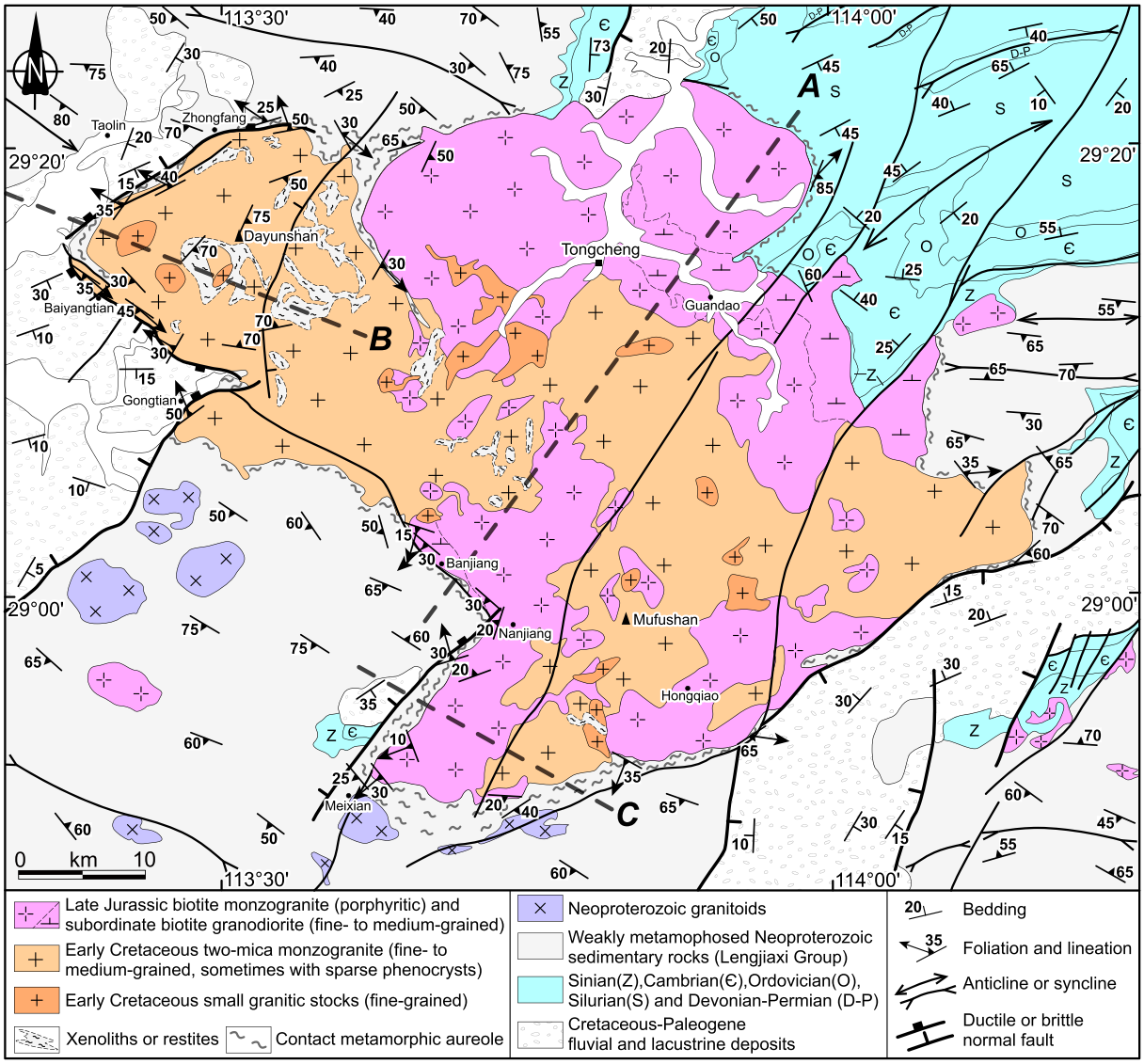

Figure 2. Geological and structural map of the Dayunshan–Mufushan area.

two-mica granitic pluton derived from crustal melting; the upper plate consists of Cretaceous–Paleogene red conglomerates and sporadic Proterozoic metasedimentary rocks, which is cut by a series of domino-style normal faults; an arc-shaped detachment fault separates the above two units. These preliminary studies provide an additional clue to address the aforementioned issues on the Late Mesozoic tectonics of South China. In this study, we conducted an integrated multidisciplinary investigation including structural geology, geochronology, anisotropy of magnetic susceptibility (AMS), and gravity methods on the Dayunshan–Mufushan batholith to decipher the multiple emplacement processes of the diachronous intrusions. The relationships between emplacement modes and regional tectonics are discussed. In order to describe our new results in detail, the work has been divided into two parts. This paper (Part 1) focuses on structural analysis and geochronological constraints, while magnetic fabrics and gravity survey are presented in a companion paper (Part 2, Ji, Chen, et al., 2017).

2. Geological Overview of the SCB

The SCB consists of the Yangtze Block in the northwest and the Cathaysia Block in the southeast (Figure 1). The Yangtze Block contains Archean–Paleoproterozoic continental nucleus (e.g., the Kongling complex in the Huangling massif) surrounded by widespread Neoproterozoic metasedimentary and igneous rocks,

whereas the Precambrian basement is sporadically exposed in the Cathaysia Block (S. Gao et al., 2011; X. H. Li, Li, & Li, 2014; Qiu et al., 2000; Yu et al., 2010). These two blocks were amalgamated along the Jiangnan orogen before ca. 820 Ma, although the subduction–collision processes are still controversial (e.g., Charvet et al., 1996; Li et al., 2009; X. L. Wang et al., 2014; Zhao, 2015; Zhao et al., 2011). The Jiangshan–Shaoxing fault along with its possible southwestward extension (i.e., the Chenzhou–Linwu fault) is generally considered as the Neoproterozoic suture zone, despite repeated reactivation by younger event. The basement rocks presently exposed in the Jiangnan domain are dominated by a thick pile of weakly metamorphosed (greenschist facies) Neoproterozoic strata with features of turbidite sequences. They have been given several names in different provinces, such as the Xikou, Shuangqiaoshan, Lengjiaxi, Fanjingshan, and Sibao Groups. These basement sequences were intruded by ca. 820 Ma late orogenic granitoids (Li et al., 2003; X. L. Wang et al., 2013; Zhao et al., 2013). After ca. 820 Ma, continental rifting led to the development of the Nanhua rift within the SCB (J. Wang & Li, 2003). Rift-related clastic sedimentary rocks represented by the Neoproterozoic Banxi Group and its equivalents unconformably overlie the folded basement sequences. This mid-Neoproterozoic angular unconformity is generally regarded as the response to the final amalgamation of the Yangtze and Cathaysia blocks.

During the Phanerozoic, the SCB experienced three main tectonothermal events in the Early Paleozoic, Early Mesozoic, and Late Mesozoic (for a review, see Y. J. Wang et al., 2013). The Early Paleozoic event is well documented along the Wuyi–Yunkai belt in the Cathaysia Block, indicated by pre-Devonian folds and thrusts, amphibolite facies to locally granulite facies metamorphism, and associated crustal melting (e.g., Charvet et al., 2010; Faure et al., 2009; Li et al., 2010; Lin, Wang, & Chen, 2008; Shu et al., 2014). This event is interpreted as an intracontinental orogeny, which closed the Nanhua rift. Structural analysis reveals a positive flower pattern for the Early Paleozoic orogen, with north- and south-directed structures rooted in the Jiangshan–Shaoxing fault. The prominent and extensive orogeny in South China took place in the Early Mesozoic. Almost contemporaneously, the SCB collided with the NCC to the north and the Indochina Block to the south, corresponding to the closure of the eastern branches of Paleo-Tethys (Dong et al., 2011; Faure et al., 2014, 2016; Wu & Zheng, 2013). Furthermore, another intracontinental orogeny involved the Xuefengshan–Jiuling belt in the central SCB that superposed upon the preexisting Jiangnan orogen, characterized by top-to-the-NW ductile shearing, folding, and thrusting of the Neoproterozoic to Early Triassic rocks and late orogenic (ca. 230–215 Ma) magmatism (Chu, Faure, Lin, & Wang, 2012; Chu, Faure, Lin, Wang, & Ji, 2012; Chu & Lin, 2014; Chu, Lin, et al., 2012). The Late Mesozoic especially the Early Cretaceous tectonics of the eastern SCB was dominated by an overall extensional tectonic regime, as manifested by the development of several domal structures (Figure 1 and the references therein) and numerous extensional basins usually controlled by normal faults (J. H. Li et al., 2014; Shu et al., 2009; D. Z. Wang & Shu, 2012), as well as the occurrence of A-type granites (Jiang et al., 2009, 2011; Li, 2000; Wong et al., 2009; Wu et al., 2012; Yang et al., 2012). On the contrary, the western SCB seems to be dominated by a compressional regime during the Late Mesozoic, particularly the regions surrounding the Sichuan basin (see section 1).

3. Structural Analysis of the Dayunshan–Mufushan Batholith

3.1. Lithological Units and Bulk Architecture

The country rocks of the Dayunshan–Mufushan batholith are composed of the Neoproterozoic Lengjiaxi Group and the Sinian (late Neoproterozoic) to Permian strata (Figure 2). The Lengjiaxi Group, mainly consists of slightly metamorphosed sandstone, siltstone, and slate, was traditionally considered to be Mesoproterozoic in age (Gu et al., 2002; Xu et al., 2007). However, recent U–Pb dating of detrital zircons as well as tuff layers from this sequence have demonstrated that its deposition occurred during ca. 860–820 Ma (L. Z. Gao et al., 2011; Meng et al., 2013; W. Wang et al., 2013; X. L. Wang et al., 2014; Yan et al., 2015). The Sinian to Permian strata are mostly distributed to the northeast of the batholith and mainly consist of carbonate and siliciclastic rocks in a shallow marine environment. All these rocks were strongly folded with two main sets of fold axes, that is, NE–SW trending and nearly W–E trending, indicative of polyphase deformation before batholith emplacement. In agreement with the previous work by Chu and Lin (2014), we consider that the regional NE-trending folding at a relatively shallow level was ascribed to the Triassic intracontinental orogeny along the Xuefengshan–Jiuling belt. The nearly W–E trending structures with pervasive slaty cleavage that developed mainly in the Neoproterozoic metasedimentary rocks are unconformably overlain by Middle Devonian conglomerate in neighboring area, indicating a pre-Devonian age

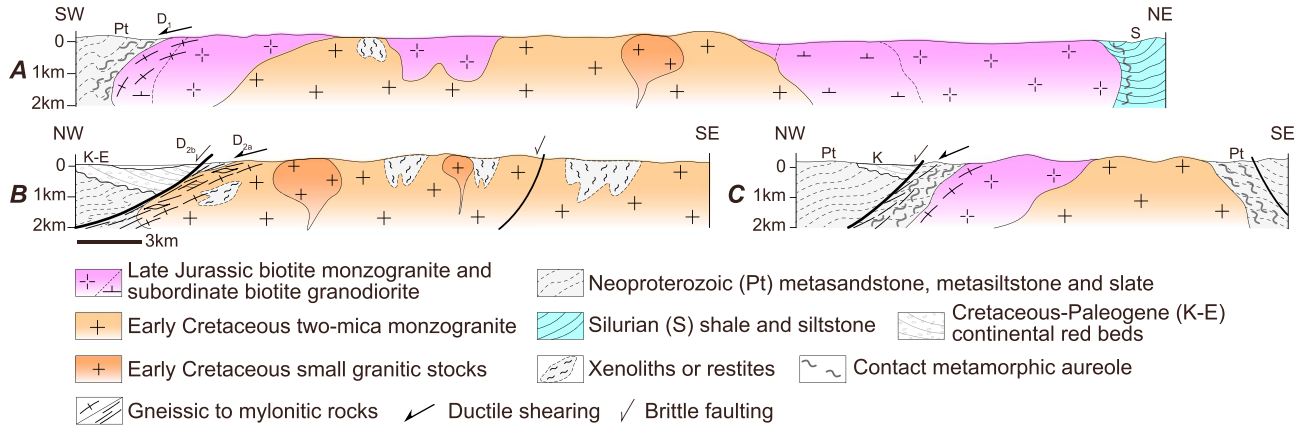

Figure 3. Geological cross-sections across the Dayunshan–Mufushan batholith (locations see Figure 2).

for this earlier episode of deformation. In addition, two NE-striking fault basins filled with Cretaceous–Paleogene alluvial and lacustrine deposits are distributed respectively on the western and southeastern sides of the batholith.

The Dayunshan–Mufushan batholith occurs as an irregular lozenge in map view, with a total outcrop area of about 2,440 km^2 (Figure 2). It mainly consists of an early-stage biotite-rich intrusion and a late-stage two-mica intrusion. Lithologically, the former is mainly composed of porphyritic biotite monzogranite and subordinate fine- to medium-grained biotite granodiorite (in the Guandao and Banjiang areas), while the latter is mostly composed of fine- to medium-grained two-mica monzogranite, sometimes with sparse phenocrysts. Both the intrusions are peraluminous, with geochemical features similar to S-type as well as fractionated S-type granites (Ji, Lin, Faure, Chen, et al., 2017). The original continuity of the nearly N–S to NE–SW trending early-stage intrusion was broken up by the emplacement of the NW–SE trending late-stage intrusion. Finally, several fine-grained small stocks of biotite or two-mica monzogranite have intruded the previous facies (Figure 3). According to geochemical analyses and LA-ICPMS zircon U–Pb dating, X. L. Wang et al. (2014) suggested that the entire batholith was formed by prolonged fractional crystallization of felsic magma during 152–146 Ma. However, our recently published SIMS zircon U–Pb ages demonstrate that the Dayunshan–Mufushan batholith was crystallized during two distinct magmatic phases with an interval of about 20 Myr. The early-stage intrusion yielded crystallization ages of 151–149 Ma, while the late-stage intrusion and the latest stocks emplaced at ca. 132 Ma and ca. 127 Ma, respectively (Ji, Lin, Faure, Chen, et al., 2017).

An approximately 200 m to 2 km wide contact metamorphic aureole was developed around the batholith, where hornfels and schists that were formed by thermal metamorphism of the Lengjiaxi Group are predominant (Figure 2). Andalusite is commonly observed in the hornfels, whereas garnet and/or staurolite can be locally found in the schists. The extent of thermal metamorphism depends significantly on the attitude of batholith–country rock interface. Schistosity in the contact zone is usually parallel to the pluton margin. Some tight, upright to recumbent folds in the host rocks close to the batholith might be the result of ductile shortening in order to create space for pluton emplacement (Figure 3). In addition, an impressive amount of small and large xenoliths or restites of relatively high-grade metasedimentary rocks (e.g., garnet-sillimanite-bearing schist) is particularly abundant in the Dayunshan massif. The xenolithic blocks of host rocks were probably captured by stoping during magma ascent.

Based on structural observations of the batholith and its country rocks at macrostructural, mesostructural, and microstructural scales, we identified two deformation events (referenced to as the early deformation D_1 and the main deformation D_2) related to batholith emplacement and subsequent exhumation.

3.2. The Early Deformation (D_1)

At the southern border of the batholith, mainly in the areas of Banjiang, Nanjiang, Meixian, and to the south of Hongqiao, the early-stage intrusion (predominantly porphyritic biotite monzogranite with a small amount

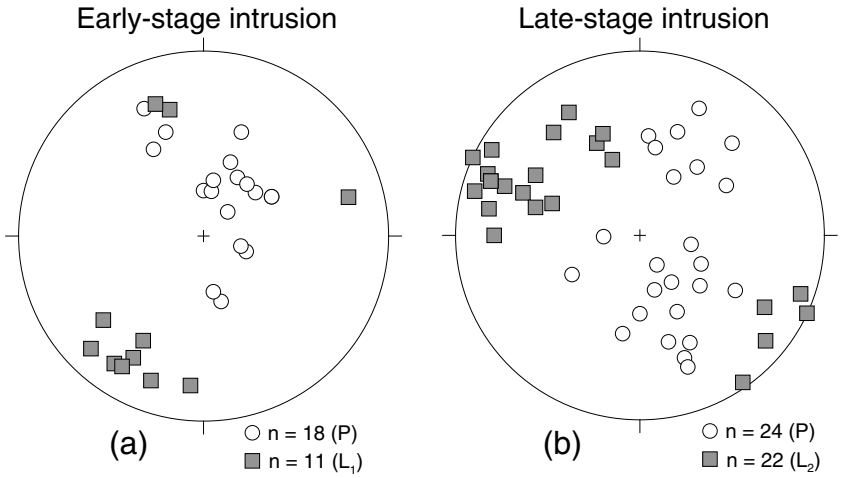

Figure 4. Equal-area projections (lower hemisphere) of the planar (P, pole to the foliation) and linear (L, lineation) structural elements from: (a) early-stage intrusion (biotite monzogranite and subordinate granodiorite) and its contact zone (mainly at the southern border of the batholith) and (b) late-stage intrusion (two-mica monzogranite) and its contact zone (mainly along the Dayunshan detachment fault).

of biotite granodiorite) was ductilely deformed at various degrees, showing a weak to locally pervasive gneissic foliation (Figures 2 and 3). The gneissosity gradually disappears away from the pluton margin, and an apparently isotropic texture is prevalent inside the pluton interior. This indicates that the deformation occurred during and slightly after the pluton emplacement. Foliation in the gneissic granite mainly dips to the SW or S, with dip angles concentrated at 20°–35° (Figures 4a and 5a). At some localities, a NE–SW trending mineral and stretching lineation (L_1) defined by alignment of quartz grains, K-feldspar phenocrysts, or biotite clots is well developed (Figures 4a and 5b). Along this L_1, asymmetric K-feldspar

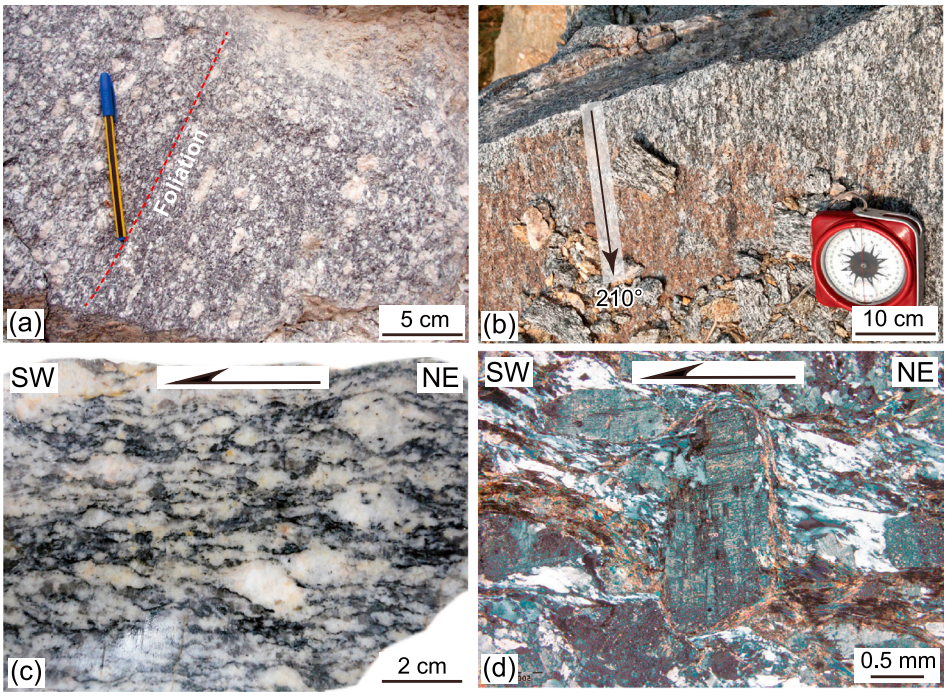

Figure 5. Structural features related to D_1 deformation in the early-stage intrusion. (a) Foliated biotite monzogranite with aligned K-feldspar phenocrysts. (b) NE–SW trending lineation in gneissic biotite granodiorite (near Banjiang). (c) Sigmoid K-feldspar phenocrysts in gneissic biotite monzogranite (near Meixian). (d) Sigma-type K-feldspar porphyroclast in mylonitic biotite monzogranite (near Nanjing) indicates a top-to-the-SW sense of shear.

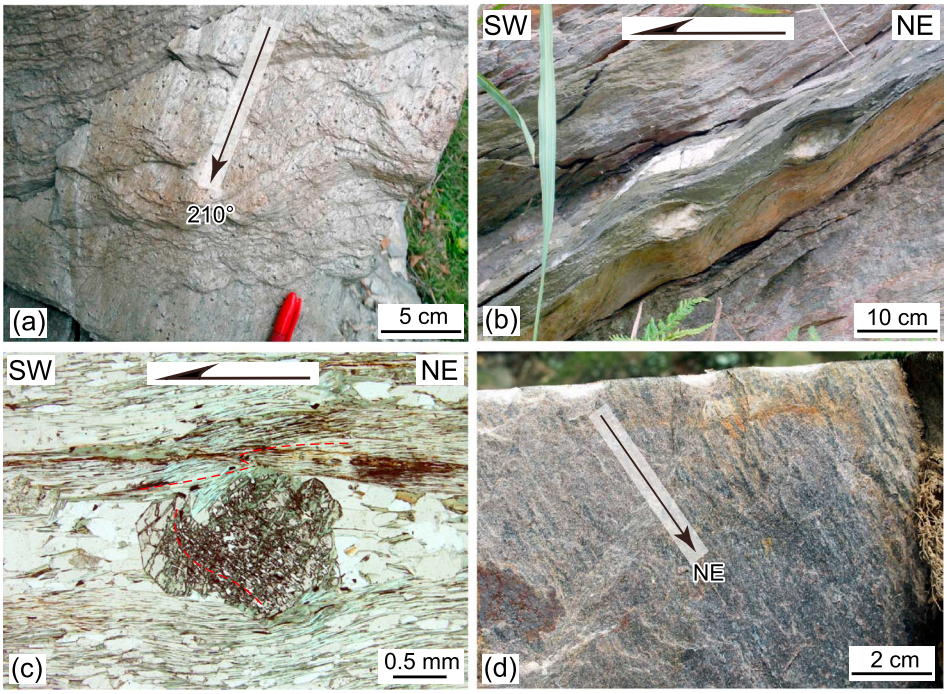

Figure 6. Structural features related to D_1 deformation in the country rocks. Figures 6a, 6b, and 6c are all from contact zone at the southeastern border of the batholith (to the south of Hongqiao). (a) NE–SW trending lineation in garnet-bearing schist. (b) Sheared felsic lenses at outcrop. (c) Sigmoid inclusion trails in garnet and asymmetric microfold of mica in thin section consistently indicate a top-to-the-SW sense of shear. (d) NE–SW trending lineation formed by andalusite in contact zone at the northeastern border of the batholith.

megacrysts or occasionally sigma-type K-feldspar porphyroclasts in the deformed granite indicate a top-to-the-SW sense of shear (Figures 5c and 5d). In general, the batholith–country rock interface at the southern border dips gently outward; hence, the contact zone becomes relatively wide (up to ~2 km). Meanwhile, the amount of garnet increases in the contact schist of this area. To the south of Hongqiao, the L_1 is quite conspicuous in the garnet-bearing schist (Figure 6a), and sheared quartz lenses in the deformed schist show a top-to-the-SW displacement (Figure 6b). Such a kinematics is further confirmed by microscopic observation of oriented thin sections of the host schist, which exhibits sigmoid inclusion trails in garnet and asymmetric microfold of mica (Figure 6c).

The northern part of the early-stage intrusion (biotite-rich monzogranite and granodiorite) appears to be mostly isotropic, lacking of planar and linear structures at outcrops. The main granite-forming minerals, namely, quartz, plagioclase, K-feldspar, and biotite, have generally euhedral to subhedral habitus without obvious preferred orientation. In other words, there is no evidence for postsolidus plastic deformation. At the northeastern border of the batholith, the contact between the pluton and the country rocks is more tortuous and steep, cutting across the bedding of the Early Paleozoic limestone, shale, and siltstone (Figures 2 and 3). A narrow contact zone with marble and hornfels was developed in this area. Locally, a NE-trending mineral lineation with downdip plunge or moderate pitch was observed on the steeply dipping foliation of the andalusite-bearing hornfels, yet no kinematic indicator was revealed by our investigation (Figure 6d).

3.3. The Main Deformation (D_2)

3.3.1. Ductile Shearing (D_{2a})

Along the western border of the batholith, an arched ductile shear zone (in map view) overprinted by brittle faults is well exposed in the areas from Zhongfang to Baiyangtian (Figures 2 and 3). This high-strain zone about 35 km in length was interpreted as a detachment fault by previous workers (Li & Yu, 1991; Yu, Ye, & Peng, 1998) here named the Dayunshan detachment fault. Mylonites in the shear zone derive mostly at the expense of the two-mica monzogranite from the late-stage intrusion. In the deformed granite, the foliation strike is generally parallel to the pluton margin, dipping at low to moderate angles (20°–50°) to the NW

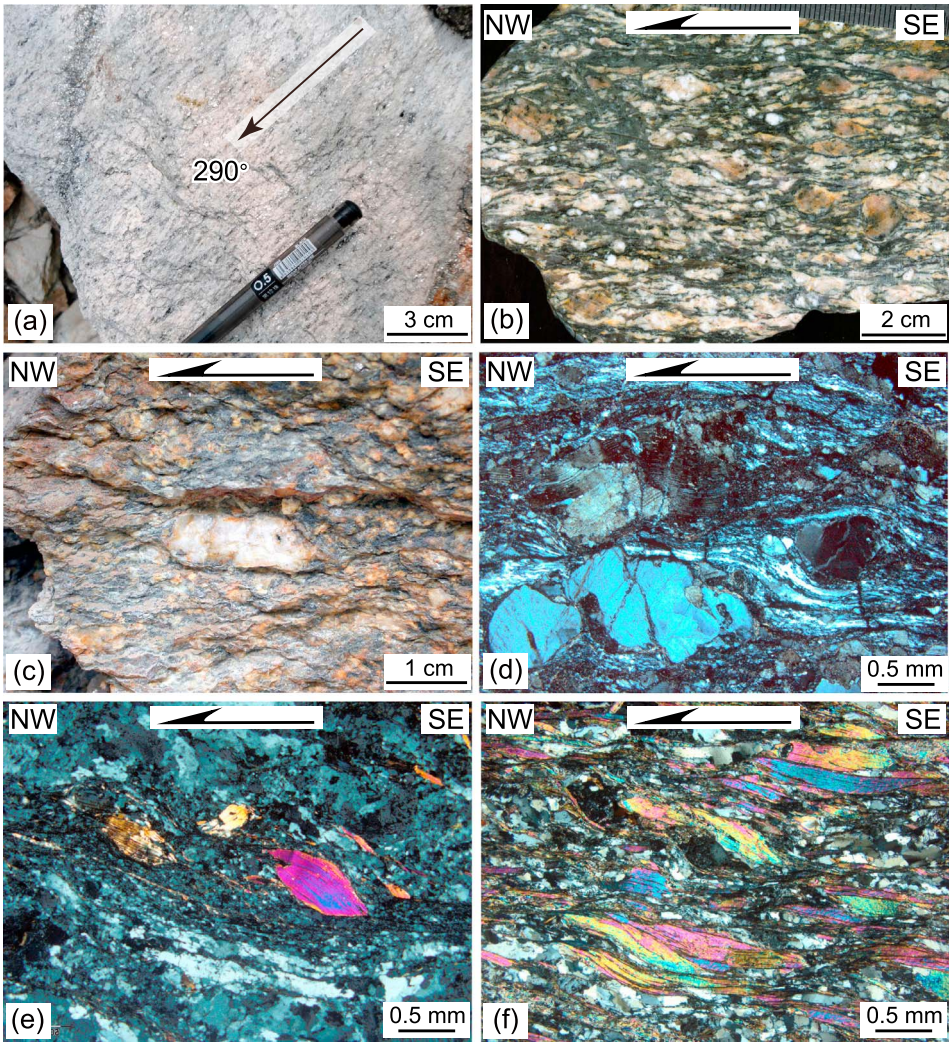

Figure 7. Structural features related to the D_{2a} ductile shearing along the Dayunshan detachment. (a) NW–SE trending lineation in albitized two-mica monzogranite. Kinematic indicators such as (b) S-C fabrics, (b, c, d) sigma-type feldspar porphyroclasts, and (e) mica fishes in granitic mylonites consistently indicate a top-to-the-NW shearing. (f) The restitic schist close to the detachment fault showing the same top-to-the-NW sense of shear.

and SW, respectively, along the two sides of the pluton (Figure 4b). In spite of the strike variation of foliation, the mineral and stretching lineation (L_2) keeps a similar NW–SE trend (Figure 4b). On the mylonitic foliation, the L_2 is usually marked by the preferred orientation of mica flakes and quartz–feldspar aggregates (Figure 7a). A consistent top-to-the-NW sense of shear is unambiguously determined by various shear criteria observed at outcrops or in thin sections of the mylonitic granites, such as S-C fabrics, sigma-type porphyroclast systems with asymmetric tails, and mica fishes (Figures 7b–7e). The top-to-the-NW shearing is also identified in the restitic schist xenoliths in the deformed granite, under the form of mica fishes confined between shear bands (Figure 7f). In addition, sporadic metasedimentary rocks of the Lengjiaxi Group exposed along the Dayunshan detachment fault are partly mylonitized, forming discontinuous narrow stripes of sericite-chlorite–quartz schist juxtaposed against the mylonitic granite. Kinematic indicators associated with the NW–SE trending lineation in the schist attest to the same top-to-the-NW sense of shear (Figures 8a and 8b).

A continuous transition from mylonitic to isotropic granite is observed across the Dayunshan detachment. The internal part of the Dayunshan massif, belonging to the western part of the late-stage intrusion, commonly shows isotropic features in the field. Locally, a magmatic layering outlined by biotite-rich schlieren develops in the places where xenoliths or restites are abundant. Similarly, there is no obvious deformation in the eastern part of the late-stage intrusion. In spite of the lack of mesoscopic structures, our AMS data reveal a

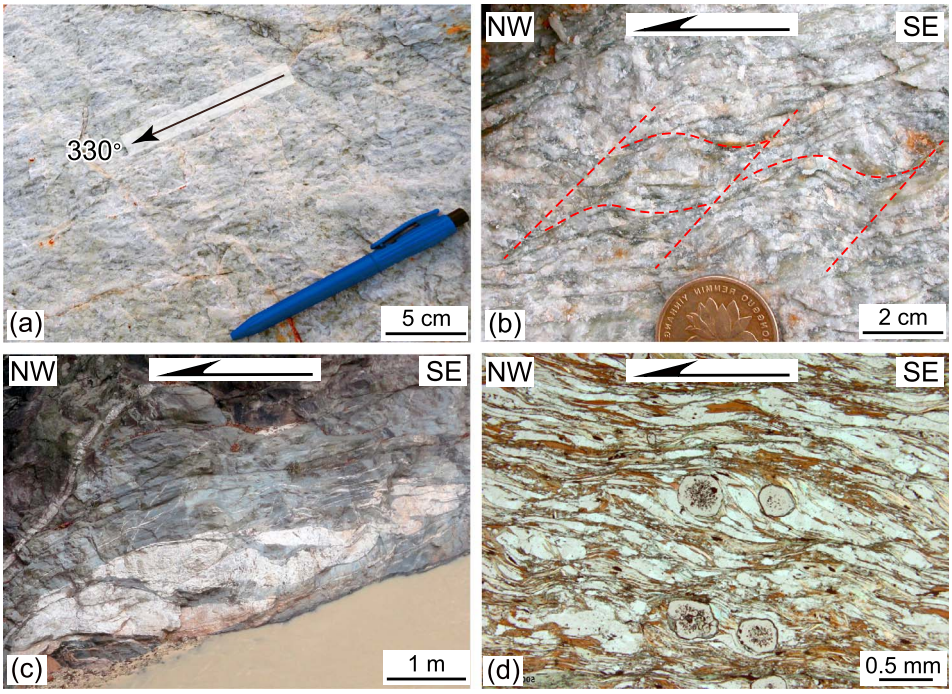

Figure 8. Structural features related to the D_{2a} ductile shearing in the country rocks. (a) NW–SE trending lineation, and (b) shear bands in a sericite–chlorite–quartz schist near Gongtian, indicating a top-to-the-NW shearing. Both Figures 8c and 8d are from the contact zone to the southwest of Nanjiang, cutting by a NE-trending ductile-brittle fault. (c) Sheared pegmatite veins within the contact schist and (d) shear bands in thinsection of the garnet-bearing schist show the same top-to-the-NW sense of shear.

predominant WNW–ESE trending magnetic lineation for the main apparently undeformed body of the late-stage intrusion, which is consistent with the observed lineation in the mylonitic granite (cf. Part 2).

It is worth noting that the D_{2a} ductile shearing is not restricted to the Dayunshan detachment fault, which is also locally developed along some NE-trending faults in the southern part of the study area. For example, to the southwest of Nanjiang, a weak L_2 was observed in a garnet-bearing schist of the contact zone cut by a ductile-brittle fault (Figures 2 and 3). Along a NW–SE traverse, pegmatite veins hosted in the schist were strongly sheared with a top-to-the-NW sense (Figure 8c). In oriented thin section of the schist, the presence of shear bands also indicates the same sense of shear (Figure 8d).

3.3.2. Brittle Faulting (D_{2b})

The Dayunshan detachment also experienced a brittle phase. Preexisting foliations of the high-strain shear zone are overprinted by moderate- to high-angle brittle faults. In thin sections of the mylonitic rocks, the feldspar and quartz grains are often cut by microfractures or microfaults, revealing a superimposed brittle event (Figure 7d). A few-meter-thick layer of chloritized and silicified breccia to cataclasite is observed in the fault zone (Figures 9a and 9b). The slickensides of the fault zone exhibit downdip striations with a normal sense of shear (Figures 9a and 9c). To the southwest of Gongtian, the possible prolongation of the Dayunshan detachment fault is gradually replaced by a NW-dipping high-angle normal fault (Figure 2). Overall, the fracture patterns and offset markers indicate a normal displacement for the brittle faulting.

To the west of the Dayunshan–Mufushan batholith, the eastward tilting of continental red beds in the supradetachment basin suggests that the normal faulting of the Dayunshan detachment was coeval with sediment infilling. Pebbles of slate and both deformed and undeformed two-mica monzogranite are ubiquitous in the Upper Cretaceous conglomerate (Figure 9d). In addition, the proportion of granitic pebbles increases progressively when approaching the detachment fault. Tectonically, this supradetachment basin partly belongs to a secondary depression of the Jianghan basin that is a large Cretaceous–Cenozoic rift basin in the middle Yangtze region (Figure 1). Similarly, a SE-dipping normal fault has controlled the development of half-graben basin to the southeast of the batholith. This conclusion is consistent with the observation that the apexes of the alluvial fans in the basin are predominantly located near the boundary fault.

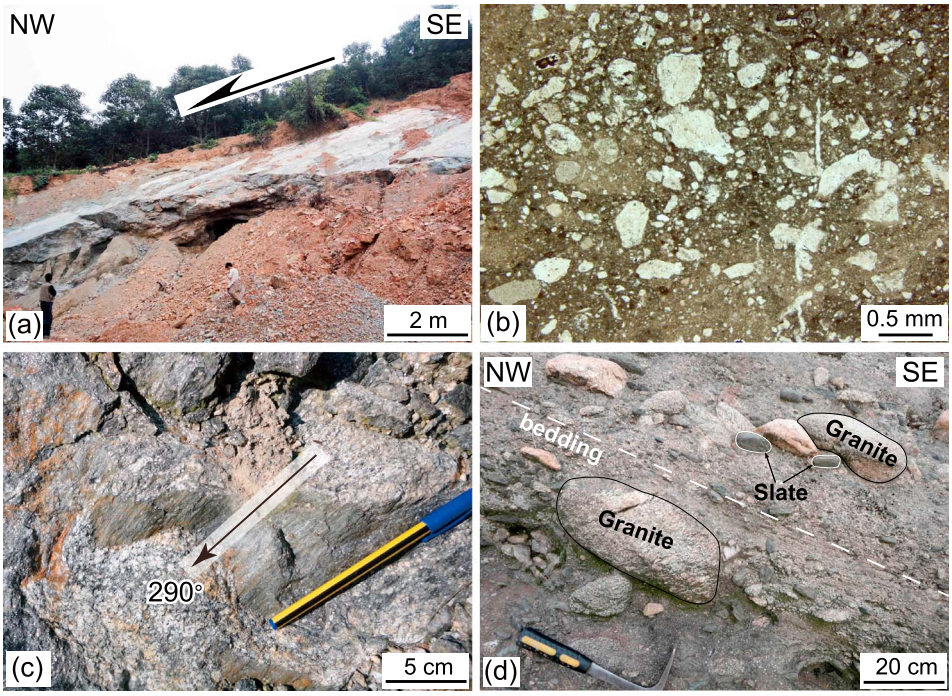

Figure 9. Structural features related to the D_{2b} brittle faulting. (a) Exhumed surface of the Dayunshan detachment fault with a few-meter-thick layer of cataclastic rocks. (b) Photomicrograph of the cataclasite from the detachment fault. (c) NW–SE trending semipenetrative striations in mica-rich facies of the two-mica monzogranite. (d) Upper Cretaceous conglomerate with pebbles of slate and granite in the supradetachment basin, Taolin area.

4. Geochronological Constraints

In order to constrain the timing of the polyphase deformation and further to reveal the thermal history of the batholith, monazite U–Th–Pb chemical and mineral $^{40}Ar/^{39}Ar$ datings have been carried out.

4.1. Monazite U–Th–Pb Chemical Dating

One deformed granite (QD69) and two mica schists (DM26 and DYS22) were collected in the study area for monazite U–Th–Pb chemical dating by electron probe microanalysis (EPMA). Obviously, in situ analysis is more effective to understand the age in relation to the petrographic context. In thin section, monazite grains were investigated directly by scanning electron microprobe in backscattered electron (BSE) mode. This allows avoiding the altered domains and inclusions. The selected grains were analyzed along linear transects using a Cameca SX-50 electron microprobe cooperated by the Institut des Sciences de la Terre d'Orléans (ISTO) and the Bureau de Recherches Géologiques et Minières in France. The analytical procedure for chemical dating was described in Cocherie et al. (1998). Accordingly, the calculated detection limit (2σ) is 150 ppm for Pb, U, and Th; this value is also taken as the absolute error. A systematic relative error of 2% is considered for Th and also for U concentrations above 7500 ppm to avoid an unrealistic low error for U-enriched grains. Age calculations and diagrams were done by using two Microsoft Excel add-in programs, namely, EPMA dating (Pommier, Cocherie, & Legendre, 2002) and ISOPLOT (Ludwig, 2003). The principles for data processing were illustrated in Cocherie and Albarède (2001). Individual analyses with poor quality were rejected according to their major oxide composition and maximum acceptable errors.

Sample QD69 is a porphyritic biotite monzogranite from the early-stage intrusion, collected in the southern tip of the batholith (Figures 5c and 10). The sample displays a gneissic structure with top-to-the SW sense of shear. Monazite grains in this sample are mainly included in the flaky biotite, ranging from 50 to 200 μm in size. They are mostly euhedral, a few of which seldom display growth zoning (Figure 11). One hundred and forty analyses were performed on seven grains. Since the results show a relatively wide range of Th/U radios, the Th/Pb versus U/Pb diagram is applicable (Cocherie & Albarède, 2001). The two intercept ages are indistinguishable within errors, and a theoretical isochron age is defined at 151.4 + 3.7/−3.5 Ma

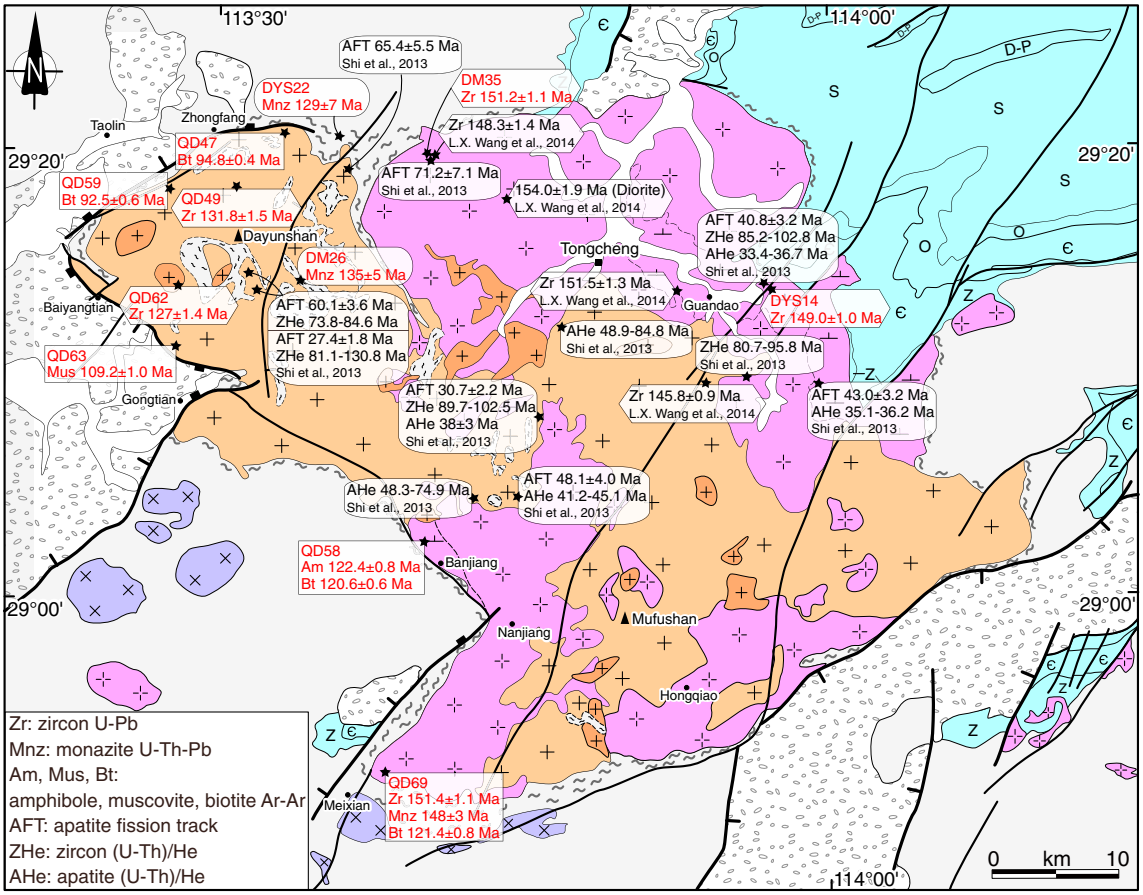

Figure 10. Available geochronological data from the Dayunshan–Mufushan batholith. The dated samples by our work (Ji, Lin, Faure, Chen, et al., 2017; this study) are in red font.

(Figure 12a). This age is equal to the zircon U–Pb age of this sample (151.4 ± 1.1 Ma; Ji, Lin, Faure, Chen, et al., 2017). Meanwhile, all the analyses yield a weighted mean age of 147.8 ± 3.4 Ma (Figure 12b). Considering that the closure temperature for Pb diffusion in monazite may be slightly lower than that in zircon (Parrish, 1990), we choose the age of ca. 148 Ma to constrain the thermal history (see below).

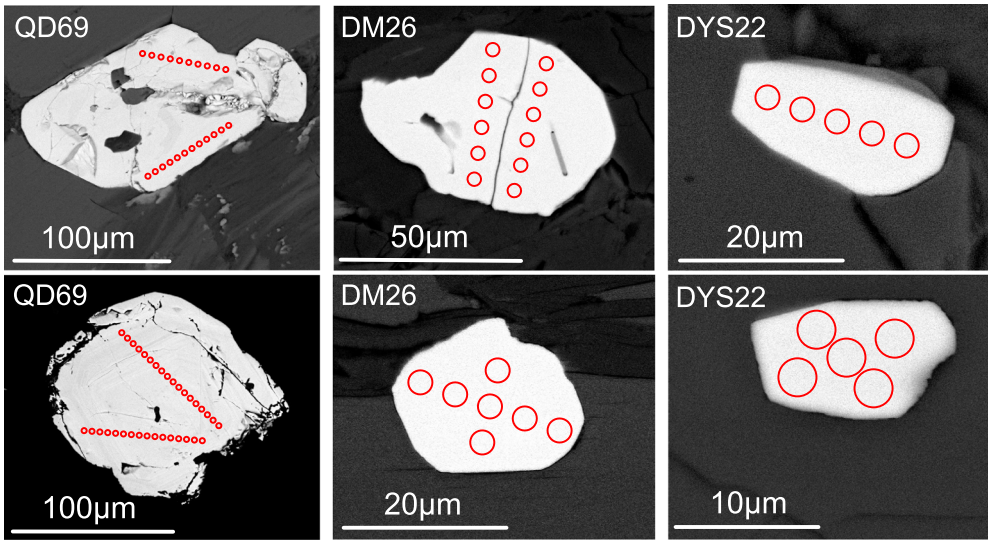

Figure 11. Representative BSE images of monazite grains in thin sections of the dated samples (for locations, see Figure 10). The circles indicate the analytical spots.

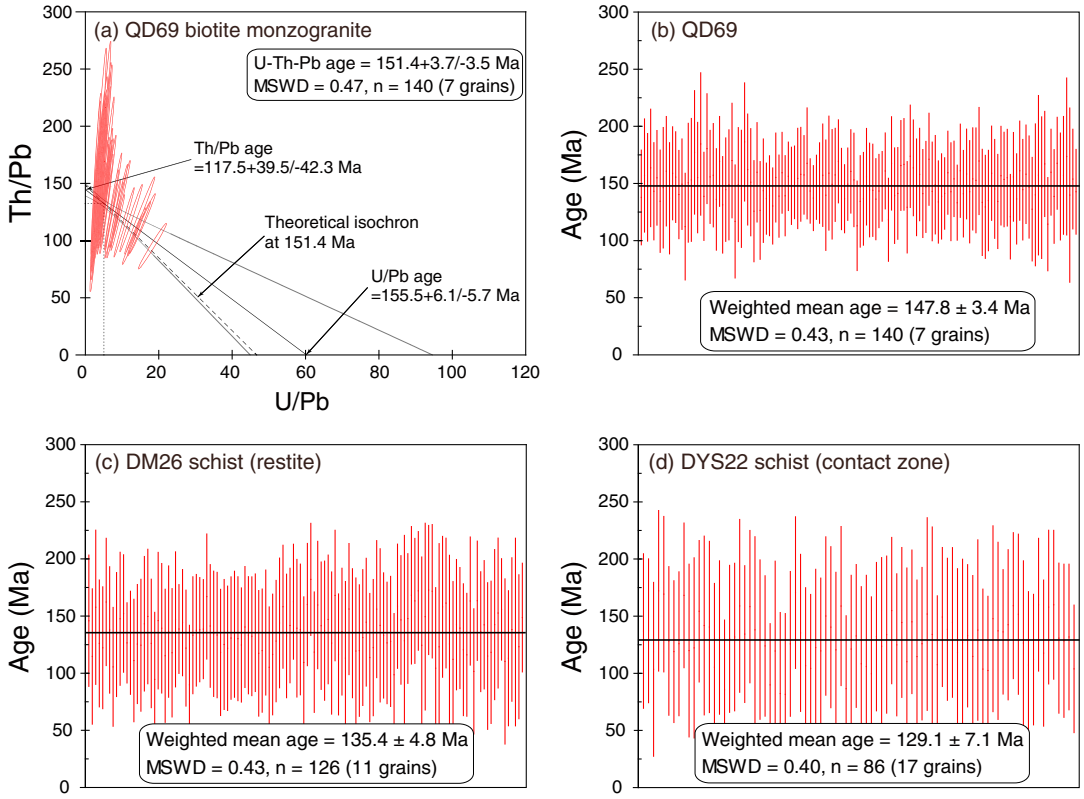

Figure 12. Monazite U–Th–Pb ages of the dated samples (locations see Figure 10). (a, b) QD69, gneissic biotite monzogranite from the early-stage intrusion. (c) DM26, sillimanite-bearing schist of restite within the late-stage intrusion. (d) DYS22, garnet-bearing schist from contact aureole of the late-stage intrusion.

Sample DM26 is a sillimanite-bearing schist collected from the central part of the Dayunshan massif, representing the restite within the late-stage intrusion (Figure 10). In the BSE images, most monazite grains in this sample are subhedral to anhedral with grain sizes of about 20–50 μm and show a homogenous texture without any zonation (Figure 11). One hundred and twenty-seven analyses on 11 grains yield a weighted mean age of 135.4 ± 4.8 Ma (Figure 12c). Taking into account the errors, this age is comparable with crystallization age of the late-stage intrusion (131.8 ± 1.5 Ma; Ji, Lin, Faure, Chen, et al., 2017). Restites in the peraluminous (or S-type) granite are probably residual from the source rocks after partial melting (Chappell, White, & Wyborn, 1987). Thus, we speculate that the crustal melting responsible for the generation of the late-stage intrusion begun no earlier than ca. 135 Ma.

Sample DYS22 is a garnet-bearing schist collected from the contact zone at the embayed border to the north (Figure 10). In the field, a NW–SE trending lineation was observed in the rock. Monazite grains occur as about 10–30 μm inclusions both in mica and quartz (Figure 11). Most of them are prismatic, with long axes parallel to the orientated mica flakes and quartz grains. Eighty-seven analyses on 17 grains yield a weighted mean age of 129.1 ± 7.1 Ma (Figure 12d). This age is interpreted as the timing of monazite growth due to thermal metamorphism associated with the emplacement of the late-stage intrusion.

4.2. $^{40}Ar/^{39}Ar$ Dating

Mica and/or amphibole were separated from gneissic or mylonitic granites for $^{40}Ar/^{39}Ar$ dating by step-heating technique. The mineral samples were irradiated in the nuclear reactor at the China Institute of Atomic Energy (Beijing). Thereafter, the $^{40}Ar/^{39}Ar$ analyses were performed using a MM-5400 mass spectrometer at the Institute of Geology and Geophysics, Chinese Academy of Sciences (IGGCAS, Beijing). Detailed sample processing and analytical procedure were described in Wang et al. (2006). The measured isotopic ratios were corrected for system blanks, mass discrimination, and irradiation-induced interference. Plateau, inverse isochron and total fusion ages with uncertainties at 2σ were calculated using the ArArCALC

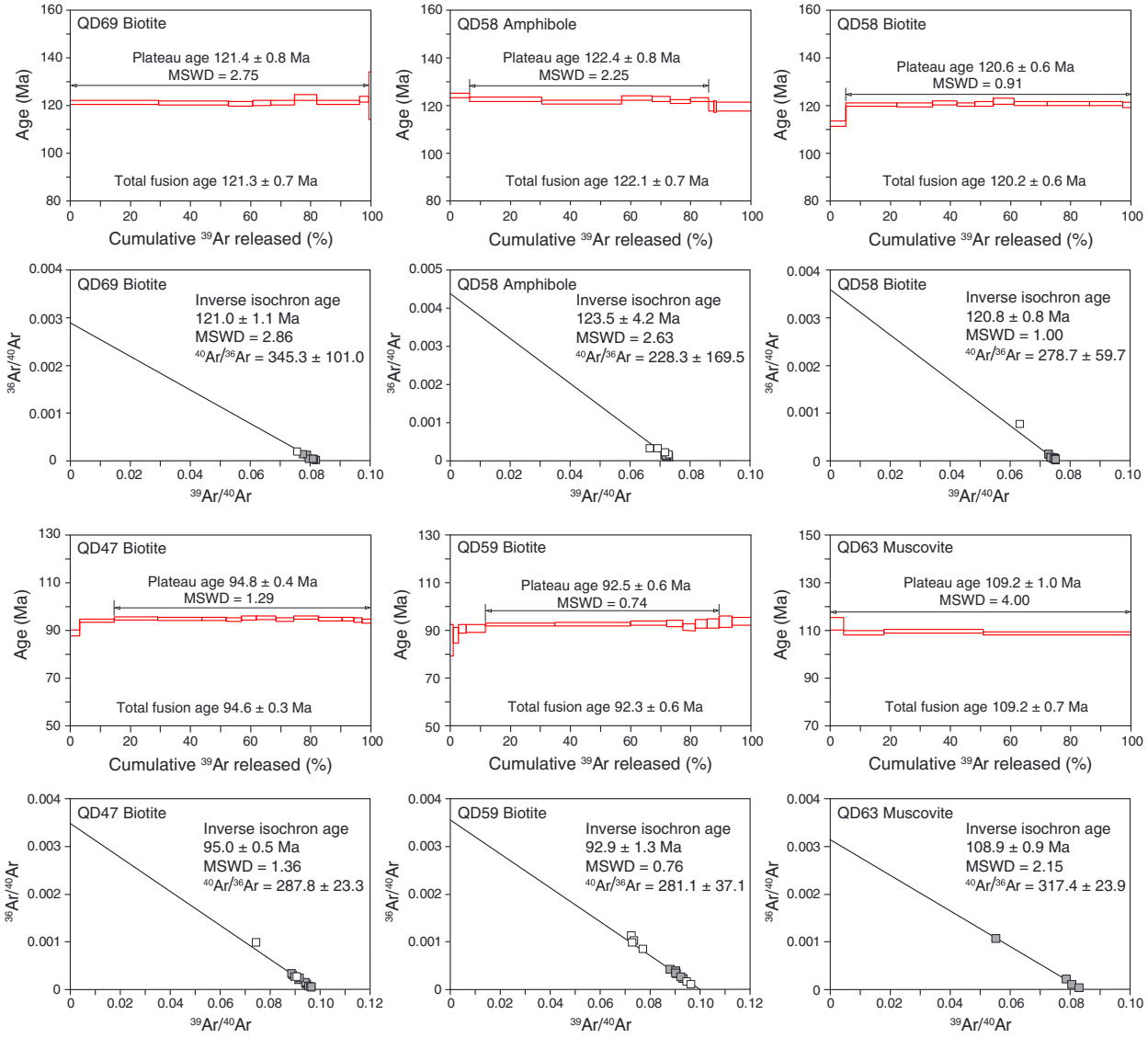

Figure 13. $^{40}Ar/^{39}Ar$ age spectra and reverse isochron plots of the dated samples (locations see Figure 10). QD69 and QD58 are gneissic granites from the early-stage intrusion, while QD47, QD59, and QD63 are mylonitic granites from the late-stage intrusion.

software (Koppers, 2002). The analytical data are reported in Table S1; the age spectra and reverse isochron plots are shown in Figure 13.

As to the early-stage intrusion, two gneissic samples were chosen for $^{40}Ar/^{39}Ar$ dating. Sample QD69 has currently been dated by both zircon U–Pb and monazite U–Th–Pb methods (Ji, Lin, Faure, Chen, et al., 2017; this study). Biotite from this sample yields a plateau age of 121.4 ± 0.8 Ma, identical to its inverse isochron age of 121.0 ± 1.1 Ma (Figure 13). Another sample QD58 is a biotite granodiorite with a pervasive foliation and a NE–SW trending lineation, collected from the southwestern margin of the batholith (near Banjiang; Figures 5b and 10). The paired amphibole and biotite from the same sample yield plateau ages of 122.4 ± 0.8 Ma and 120.6 ± 0.6 Ma, respectively, in agreement with their inverse isochron ages at 123.5 ± 4.2 Ma and 120.8 ± 0.8 Ma (Figure 13). It is noteworthy that these $^{40}Ar/^{39}Ar$ ages (123–121 Ma) from different rock types of the early-stage intrusion are much younger than their crystallization ages of 151–149 Ma and even slightly postdate the emplacement of the late-stage intrusion as well as the latest stocks during 132–127 Ma (Ji, Lin, Faure, Chen, et al., 2017). Thus, we argue that the late-stage tectonomagmatism was responsible for a thermal resetting of the $^{40}Ar/^{39}Ar$ geochronometer, since there was an interval of more than 15 Myr during which the early-stage intrusion had enough time to cool down to a relatively low

temperature at the shallow crustal levels. Furthermore, the close amphibole and biotite ages with a discrepancy lower than 3 Myr indicates a rapid cooling and exhumation process at this time.

Three samples of mylonitic two-mica monzogranite from the Dayunshan detachment fault were also dated (Figure 10). In these samples, mica with a shape preferred orientation parallel to the L_2 was ductilely deformed by a top-to-the-NW shearing (Figure 7). Biotite from samples QD47 and QD59 yield two plateau ages at 94.8 ± 0.4 Ma and 92.5 ± 0.6 Ma, respectively, corresponding to inverse isochron ages of 95.0 ± 0.5 Ma and 92.9 ± 1.3 Ma (Figure 13). Muscovite from sample QD63 yields a plateau age of 109.2 ± 1.0 Ma and an inverse isochron age of 108.9 ± 0.9 Ma (Figure 13). The $^{40}Ar/^{36}Ar$ initial values of these samples range from 281 to 317, which are close to that of the present-day atmosphere. Zircon U–Pb dating of the late-stage intrusion revealed that its crystallization age is at ca. 132 Ma (Ji, Lin, Faure, Chen, et al., 2017). Therefore, these younger mica $^{40}Ar/^{39}Ar$ ages (ca. 109 Ma and 95–93 Ma) probably represent the cooling ages related to the protracted activity of the Dayunshan detachment fault through the closure temperatures of muscovite and biotite (about 400°C and 300°C, respectively; McDougall & Harrison, 1999).

5. Timing of the Deformation and Thermal History

Timing of the polyphase deformation has been the subject of numerous structural studies. Recognition of the detailed structural sequence, together with thermochronological data (e.g., $^{40}Ar/^{39}Ar$ dating of synkinematic minerals), allows us to decipher the distinct stages of tectonic evolution. However, it is crucial to establish a reasonable link between radiometric ages and microstructures directly related to the polyphase deformation. According to the closure temperature concept (Dodson, 1973), the use of different radiometric system provides a possibility to delineate the thermal history of the batholith.

At the scale of the entire batholith, D_1 was observed mostly at the southern border of the batholith (in the early-stage intrusion and along its contact zone). The microstructures of the deformed granite are dominated by submagmatic to weak solid-state deformation at high-temperature subsolidus conditions (e.g., microfractures filled by late magmatic minerals, myrmekite, undulose extinction, and weakly recrystallized quartz grains), whereas the mylonitic fabrics (i.e., strong solid-state deformation, such as porphyroclast system of K-feldspar, quartz ribbon, and mica fish) are locally present (Figure 5d; e.g., Paterson, Vernon, & Tobisch, 1989; Vernon, 2000). The continuous transition from deformation fabrics along the pluton margin to purely magmatic microstructures in the pluton interior argues for a synkinematic emplacement of the early-stage intrusion. This deduction is supported by the parallel solid-state and magmatic foliations and lineations, as revealed by the field and AMS measurements (cf. Part 2). Moreover, the syntectonic porphyroblast growth in the contact schist indicates that the deformation is coeval with the thermal metamorphism (Figures 6a and 6c). Thus, D_1 is closely related to the emplacement of the early-stage intrusion. Our zircon U–Pb and monazite U–Th–Pb datings reveal that the early-stage intrusion emplaced at ca. 150 Ma and then cooled rapidly from about 800°C down to about 725°C as indicated by the closure temperatures of zircon and monazite (Figure 14). These results also place age constraints on the D_1 event around 150 Ma.

The D_2 event can be subdivided into two phases, namely, ductile shearing (D_{2a}) and subsequent brittle faulting (D_{2b}). Ductile shearing is spectacularly developed at the western border of the batholith. The late-stage intrusion was syntectonically involved in mylonitization along the Dayunshan detachment fault. Across the main detachment, the tectonite series develops from mylonitic in the deep levels into cataclastic in the shallow ones. Such an evolution indicates a progressive deformation from ductile to brittle. Plastic deformation of feldspar and quartz in the mylonitic granite is associated with a pervasive grain-size reduction (Figures 7d and 7e). Feldspar porphyroclasts display kink bands or deformation bands, and recrystallization appears around a few subgrains. Quartz in the matrix commonly underwent intense dynamic recrystallization, forming elongate ribbons oblique to the primary foliation. These microstructural features reveal a significant solid-state deformation that might have initiated at temperatures higher than 500°C (e.g., Passchier & Trouw, 2005). Moreover, the deformation fabrics gradually weaken toward the pluton interior, and submagmatic microstructures are locally preserved despite the obscuring effects of the intensive postsolidus deformation. Also, the AMS results show consistent planar and linear fabrics from the external mylonitic granite to the internal isotropic granite (cf. Part 2). Considering the geometrical relationship between pluton and shear zone, as well as the structural coherence across the shear zone, the Dayunshan massif can thus be regarded as a syntectonic pluton emplaced during the activity of the detachment fault. Accordingly, the zircon U–Pb

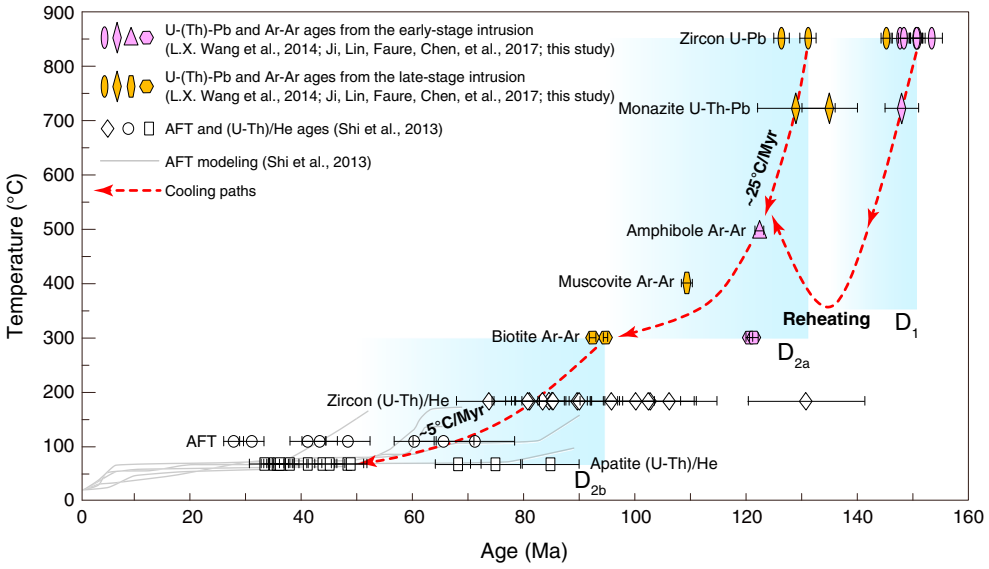

Figure 14. Cooling history of the Dayunshan–Mufushan batholith. Geochronological data (Figure 10) including zircon U–Pb (about 850°C), monazite U–Th–Pb (about 725°C), amphibole, muscovite, and biotite Ar–Ar (about 500°C, 400°C, and 300°C), zircon and apatite (U–Th)/He (about 180°C and 70°C), and AFT (about 110°C) ages are plotted at their respective closure temperatures. The speculated duration of the polyphase deformation is indicated by the shadow boxes.

and monazite U–Th–Pb ages (135–129 Ma) from the late-stage intrusion and associated metamorphic rocks constrain the onset of the D_{2a} ductile shearing. Taking into account the $^{40}Ar/^{39}Ar$ results, we suggest that the ductile deformation probably operated over a protracted period lasting until ca. 95 Ma (Figure 14). Moreover, the early-stage intrusion was largely reheated due to the emplacement of the late-stage intrusion. This is also the reason for $^{40}Ar/^{39}Ar$ age resetting of the former. A rapid cooling in response to the early phase of D_2 event is indicated by the thermal history, at an average rate of about 25°C/Myr before ca. 110 Ma.

The D_{2b} brittle faulting is difficult to date directly due to its low-temperature nature (below approximately 300°C). Nonetheless, the biotite $^{40}Ar/^{39}Ar$ ages from the Dayunshan detachment fault can be considered as the timing of transition from ductile to brittle conditions. In other words, the domination of brittle faulting in the study area occurred after 95–93 Ma. Low-temperature thermochronological data from the Dayunshan–Mufushan batholith (Shi et al., 2013), including apatite fission track and zircon or apatite (U–Th)/He ages (Figure 10), revealed an obvious but differential exhumation during 90–50 Ma (Figure 14). An average cooling rate of about 5°C/Myr can be estimated from the generalized cooling path. The Early Cretaceous Taohuashan–Xiaomoshan plutons to the northwest of the study area recorded similar thermal history with an enhanced cooling during 96–60 Ma (Shen et al., 2012). Unroofing of the Dayunshan–Mufushan batholith during this period provided massive detritus into the half-graben basins on its both sides.

6. Regional Tectonic Implications

6.1. Compressional or Extensional Setting at ca. 150 Ma?

As already mentioned before, D_1 at the southern border of the batholith is characterized by a NE–SW trending lineation and associated top-to-the-SW shearing in the early-stage intrusion and along its contact zone. This deformation phase is nearly coeval with the emplacement at ca. 150 Ma. In view of the structural features, the possibility that this event would result from the forced expansion of the late-stage intrusion can be ruled out. We infer that the process of magma ascent for the early-stage intrusion was driven by a southward transport, consistent with the kinematics of the D_1 event. Such an emplacement mode is supported by our AMS and gravity data: the main body of the early-stage intrusion yields predominantly N–S to NE–SW trending magnetic lineations; its main feeder zone is rooted in the north (cf. Part 2). This situation is reminiscent of the Yiwülushan massif in the eastern NCC, which recorded a Late Jurassic to Early Cretaceous (around 141 Ma) compressional event before its overprinting by the development of

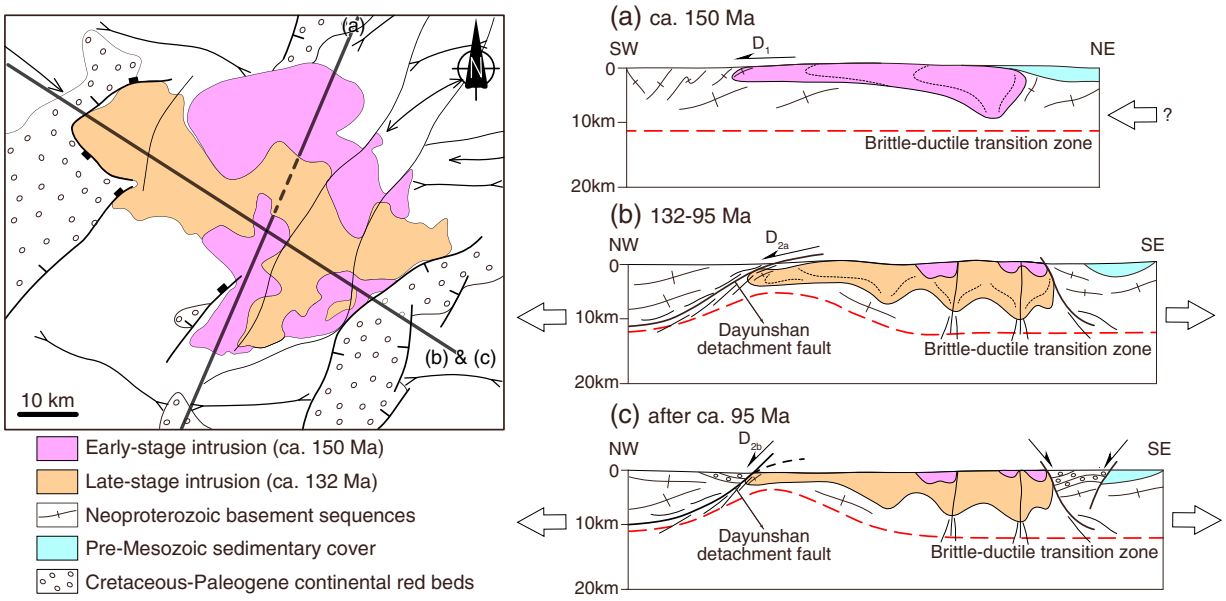

Figure 15. A possible scenario for multiple emplacement and exhumation processes of the Dayunshan–Mufushan batholith (see the plan view for positions of the NE–SW and NW–SE sections). The overlying rocks above the pluton roof are not considered, and the shape at depth of the plutons is inferred from gravity data (cf. Part 2). (a) ca. 150 Ma: Emplacement of the early-stage intrusion partially assisted by farfield compression from the north. (b) 132–95 Ma: Syntectonic emplacement and exhumation of the late-stage intrusion under a NW–SE extensional tectonic regime (featured by the top-to-the-NW Dayunshan detachment fault), which significantly reheated the early-stage intrusion. (c) After ca. 95 Ma: Brittle faulting and development of the half-graben basins on both sides of the batholith.

extensional tectonics (Lin, Charles, et al., 2013; Lin, Faure, et al., 2013). There, the early top-to-the-SW compressional structures have been clearly established by a combined AMS and gravity study of the Jurassic pluton that occupies almost half of the current Yiwülushan dome. A question is raised equally concerning the tectonic regime (e.g., compression versus extension) responsible for emplacement of the Dayunshan–Mufushan early-stage intrusion and concomitant D_1 deformation.

Several lines of research mentioned hereunder lead us to favor a distal compressional regime at ca. 150 Ma in the study area. Along the southern foreland belt of the Qinling–Dabie orogen, SW-directed folding and thrusting during the Middle Jurassic to Early Cretaceous has been well documented. This event created the Dabashan orocline to the west and the buried fold–thrust belt under the Cretaceous–Cenozoic Jianghan basin to the east (Hu et al., 2012; Li, Zhang, Dong, & Shi, 2013; Liu et al., 2015; Shi et al., 2012). At approximately the same period, the Xuefengshan belt in the central SCB propagated northwestward, forming another arcuate fold–thrust belt that converged together with the Dabashan orocline in the northeastern corner of the Sichuan basin (Liu et al., 2015; Yan et al., 2009, 2003). The aforementioned intracontinental contraction has been attributed to continued clockwise rotation and northward indentation of the SCB (i.e., the Sichuan basin behaved as a rigid block) after the Triassic North–South China collision (e.g., Meng, Wang, & Hu, 2005; E. Wang et al., 2003). The Dayunshan–Mufushan area, just located in front of the northern Yangtze foreland belt, might be also affected by the contractional tectonics. In this case, D_1 chiefly associated with the emplacement of the early-stage intrusion can be partially assisted by the farfield compression from the north (Figure 15a). It is worth noting that the regional structures of the country rocks result mainly from the tectonic events that preceded the emplacement of the batholith (Chu & Lin, 2014). This suggests that in the study area, the crustal shortening during the pluton emplacement at around 150 Ma was rather weak, since no coeval large-scale folding and thrusting have been identified in the country rocks. In other words, the emplacement process was not significantly controlled by tectonic factor. A reasonable explanation is that, in contrast with the rigid country rocks, the granitic magma as melted material was more easily affected by the distal stress field during the cooling and solidification. On the basis of our data, however, we cannot rule out an extensional emplacement mode for the early-stage intrusion. Taking a broad view to the regional tectonic framework, geological evidence in support of a very late Jurassic extensional event has been seldom documented in South China, even in the whole eastern China (Dong et al., 2015; Li et al., 2012). Furthermore, the period of ca. 150–140 Ma represents a relative "magmatic quiescence" of the SCB. Most authors consider

that the Jurassic (ca. 165–150 Ma) and Cretaceous (ca. 140–90 Ma) magmatic flare-up events in SE China were accompanied by lithospheric extension, whereas the magmatic lull during the interval likely corresponds to a short-lived compressional or transpressional setting (see Ji, Lin, Faure, Chen, et al., 2017, for a discussion). Nonetheless, more work is required to corroborate our interpretation, especially structural studies of other contemporaneous plutons.

6.2. Cretaceous Extensional Tectonics

In recent years, a number of studies have been conducted on the Late Mesozoic extensional structures (including MCCs, magmatic domes, or syntectonic plutons bounded by ductile normal faults) in North China, such as the Hohhot (Davis & Darby, 2010), Yunmengshan (Zhu et al., 2015), Yiwulushan (Lin, Charles, et al., 2013, Lin, Faure, et al., 2008, 2013), Liaodong Peninsula (Charles et al., 2012; Lin et al., 2011; Liu et al., 2013), and Jiaodong Peninsula (Charles et al., 2011, 2013). Most of these extensional structures share several common features, namely, (1) the stretching lineation in mylonites and the slickenline on fault planes document a bulk NW–SE stretching; (2) the detachment faults or brittle normal faults are characterized by top-to-the-NW or top-to-the-SE kinematics, generally with half-graben basins developed on their hanging walls; and (3) the synkinematic minerals yield $^{40}Ar/^{39}Ar$ ages concentrated mostly around 135–115 Ma (see the summary in Lin, Charles, et al., 2013). Consequently, a consensus has been reached that the NCC destruction took place under a NW–SE extensional tectonic regime during the Early Cretaceous. Similarly, the Triassic HP–UHP orogenic belt along the northern margin of the SCB (i.e., the Tongbai–Dabie–Sulu orogen) was also reworked by the same extensional event. For instance, the core of the Tongbaishan massif formed a huge extensional antiform, the Dabieshan massif was overprinted by a migmatite-cored MCC, and the southern Sulu massif was exhumed by a single detachment fault (Ji, Lin, Faure, Shi, et al., 2017; Lin et al., 2015).

In fact, several Late Mesozoic extensional massifs have also been documented in South China (Figure 1). However, the kinematic pattern and precise timing of the continental extension therein remain inconclusive. Along the Xuefengshan–Jiuling belt, a few domal structures with ductile shear zones (e.g., the Wugongshan, Lushan, and Hengshan) have been studied by previous workers. The Wugongshan massif has a typical dome shape with a long axis oriented ENE–WSW; its core consists of metamorphic pre-Devonian rocks and several generations of granitoids. It is shown that the ductile deformation in this dome initiated in the Late Triassic, with divergent motion on the shear zones along its northern and southern sides, whereas the emplacement of Late Mesozoic granitic plutons induced the thermal doming during the final stage (Faure et al., 1996). A Late Jurassic granitic pluton in the dome core, named Hukeng (154–158 Ma, zircon U–Pb dating by Wang et al., 2015), displays syntectonic features, its southern margin being ductilely deformed by a top-to-the-S shearing and the deformed granite yielding a biotite $^{40}Ar/^{39}Ar$ age of ca. 132 Ma (Faure et al., 1996). The Lushan massif exhibits as a NE-striking elongated dome, with a basal detachment separating the Neoproterozoic metamorphic basement and the overlying Neoproterozoic–Paleozoic cover to the northwest. A top-to-the-NW extensional décollement was observed in the cover, while the basement experienced ductile deformation with NNE- to WSW-trending lineations (Lin et al., 2000; Q. B. Zhu, Yang, & Wang, 2010). This main extensional event was attributed to the thermal doming induced by magmatic activity in the dome core dated at 133–126 Ma (zircon and titanite U–Pb dating). Moreover, a NNE–SSW trending ductile normal fault dated at ca. 100 Ma (mica $^{40}Ar/^{39}Ar$ ages) cut the eastern margin of the Lushan dome. Recently, Li, Zhang, Dong, Su, et al. (2013) and Li et al. (2016) conducted detailed structural and geochronological studies on the Hengshan extensional dome. Along the western margin of this dome, a top-to-the-NW detachment fault has been recognized. The dome footwall is occupied by granitic plutons composed of ca. 150 Ma monzogranite in the southwest and ca. 230 Ma granodiorite in the northeast. According to zircon U–Pb dating of a deformed albitite dyke and mica $^{40}Ar/^{39}Ar$ dating of mylonitic granites from the detachment fault, it has been suggested that the ductile shearing begun at ca. 136 Ma and lasted until ca. 97 Ma (Li, Zhang, Dong, Su, et al., 2013; Li et al., 2016). However, Wei et al. (2016) argued that the ca. 150 Ma monzogranite is syntectonic based on AMS and gravity data and thereby considered that the NW–SE extension in this area started since the Late Jurassic. Additionally, in the eastern foreland of the Dabie orogen, the NE-striking Hongzhen dome investigated by G. Zhu et al. (2010) exposes a narrow Precambrian metamorphic basement that recorded a top-to-the-SW ductile shearing. Muscovite $^{40}Ar/^{39}Ar$ dating of the mylonitic rocks from this dome yield ages of 129–126 Ma. An Early Cretaceous NE–SW extension was accordingly proposed for the dome formation. Close to the Hongzhen dome, a multidisciplinary study has been carried out on the Qingyang–Jiuhua batholith (consisting of an outer ca. 142 Ma granodiorite and an inner ca. 131 Ma

monzogranite) in the lower Yangtze River belt (Wei, Chen, et al., 2014; Wei, Martelet, et al., 2014). The results reveal that emplacement of this batholith experienced a vertical injection of the magma controlled by a NW–SE brittle stretching of the upper crust.

The abovementioned examples show that apart from the NW–SE extension as documented in the Tongbaishan, Dabieshan, Lushan, Hengshan, and Qingyang–Jiuhua massifs that complies well with the stretching direction observed in the NCC, there also seems to be N–S or NE–SW extensional massifs such as the Wugongshan and Hongzhen. Moreover, the younger $^{40}Ar/^{39}Ar$ age group (ca. 110–90 Ma) from the Lushan and Hengshan massifs indicates that the extensional deformation probably experienced a secondary or prolonged ductile phase (Li, Zhang, Dong, Su, et al., 2013; Li et al., 2016; Lin et al., 2000). Our study provides another example to address the Late Mesozoic extensional tectonics in South China. The D_2 event in the Dayunshan–Mufushan area is featured by the activity of the Dayunshan detachment fault that shows the same kinematics as the Hengshan detachment fault (Li, Zhang, Dong, Su, et al., 2013; Li et al., 2016; Wei et al., 2016). We therefore conclude that the emplacement of the Dayunshan–Mufushan late-stage intrusion at ca. 132 Ma was dominated by a NW–SE extension (Figure 15b). This is in good agreement with our gravity modeling along a WNW–ESE profile across the late-stage intrusion that indicates several linear feeder zones perpendicular to the regional stretching direction (cf. Part 2). Our $^{40}Ar/^{39}Ar$ data reveal that the ductile shearing along the Dayunshan detachment probably lasted until ca. 95 Ma, which is also synchronous with the Hengshan detachment (Li, Zhang, Dong, Su, et al., 2013, Li et al., 2016). After ca. 95 Ma, the incremental evolution of brittle faulting in the shallow crust controlled the red bed deposition in the half-graben basins and further exhumed the Dayunshan–Mufushan batholith (Figure 15c). The boundary faults of the half-graben basins in the study area strike NE, implying a continuation of the NW–SE extension during the Late Cretaceous. This is consistent with the predominantly NE-striking distribution of the other contemporaneous rift basins in southeast China (J. H. Li et al., 2014; Shu et al., 2009; D. Z. Wang & Shu, 2012).

From the regional point of view, we argue that there might be no Cretaceous N–S or NE–SW extension in the SCB. It is worth noting that the deformation features of the Jurassic pluton in the Wugongshan dome can be compared with that of the Dayunshan–Mufushan early-stage intrusion. As discussed above, we interpret the early deformation in the study area as a compressional event. We also note that the $^{40}Ar/^{39}Ar$ ages from the metamorphic basement of the Hongzhen dome are coeval with the emplacement of the nearby (~2 km) undeformed granite (Wu et al., 2012). Thus a thermal resetting of the $^{40}Ar/^{39}Ar$ system due to Cretaceous plutonism is likely, and accordingly, the ductile shearing in the Hongzhen dome might be unrelated to the Cretaceous extension. Finally, in contrast with the NCC, it seems that the overall intensity of the continental extension in the interior of South China appears to be weak. This is demonstrated by the different cooling patterns of the Yangtze craton and NCC during the Late Mesozoic; that is, the former cooled more gently than the latter (F. Wang et al., 2014). Indeed, MCC exhumation requires a larger amount of crustal stretching than syn-extensional pluton emplacement. According to our knowledge, most of the extensional domes mentioned above (including the Wugongshan, Lushan, Hengshan, and Hongzhen) are thermal domes related to plutonism, rather than MCCs as suggested by some authors (Shen, Zhang, & Zhang, 2008, and references therein). In particular, the Huangling massif belonging to the stable Yangtze craton just recorded an extension at shallow crustal level due to Cretaceous uplift and tilting (Ji et al., 2014).

7. Conclusions

The Dayunshan–Mufushan batholith provides a typical case to decipher the Late Mesozoic tectonics of South China. Based on field and microstructural observations, we have identified two deformation events related to emplacement and subsequent exhumation of the batholith. The D_1 event is characterized by a top-to-the-SW ductile shearing and closely related to the emplacement of the early-stage intrusion at ca. 150 Ma, partly in response to farfield compression of the northern Yangtze foreland belt. The D_2 event is featured by the activity of the Dayunshan detachment fault with a top-to-the-NW movement, representing the main extensional event in the study area. The late-stage intrusion can be considered as a syntectonic pluton emplaced during crustal stretching. Geochronological data (including monazite U–Th–Pb, mineral $^{40}Ar/^{39}Ar$, and our published zircon U–Pb ages) reveal that the ductile shearing (D_{2a}) along the detachment fault initiated at ca. 132 Ma and lasted until ca. 95 Ma. Subsequently, the late exhumation of the batholith was dominated by brittle faulting (D_{2b}), coeval with half-graben development on its both sides. Determination of Cretaceous NW–SE extension

in South China implies that the destruction of the NCC is not an isolated event, but an outcome of continental-scale phenomenon of East Asia.

Acknowledgments
Supplementary data related to this article can be found in the supporting information or are available by contacting the first author (e-mail: jiwenbin@mail.iggcas.ac.cn). This work has been financially supported by the MOST of China (grants 2016YFC0600401 and 2016YFC0600102) and the NSFC (grants 41502202 and 41225009). Special thanks are due to Ida Di Carlo in ISTO and also to Wenbei Shi and Fei Wang in IGGCAS for their assistance with the EPMA and Ar–Ar datings. We also thank Jean-Luc Bouchez, an anonymous reviewer, and Paul Tregoning (Editor) for their careful, critical, and constructive reviews that have greatly helped us to improve the manuscript.

References

Chappell, B. W., White, A. J. R., & Wyborn, D. (1987). The importance of residual source material (restite) in granite petrogenesis. *Journal of Petrology*, *28*(6), 1111–1138. https://doi.org/10.1093/petrology/28.6.1111

Charles, N., Augier, R., Gumiaux, C., Monié, P., Chen, Y., Faure, M., & Zhu, R. X. (2013). Timing, duration and role of magmatism in wide rift systems: Insights from the Jiaodong Peninsula (China, East Asia). *Gondwana Research*, *24*(1), 412–428. https://doi.org/10.1016/j.gr.2012.10.011

Charles, N., Gumiaux, C., Augier, R., Chen, Y., Faure, M., Lin, W., & Zhu, R. X. (2012). Metamorphic core complex dynamics and structural development: Field evidences from the Liaodong Peninsula (China, East Asia). *Tectonophysics*, *560–561*, 22–50.

Charles, N., Gumiaux, C., Augier, R., Chen, Y., Zhu, R. X., & Lin, W. (2011). Metamorphic core complex *vs*. synkinematic pluton in continental extension setting: Insights from key structures (Shandong Province, eastern China). *Journal of Asian Earth Sciences*, *40*(1), 261–278. https://doi.org/10.1016/j.jseaes.2010.07.006

Charvet, J., Shu, L. S., Faure, M., Choulet, F., Wang, B., Lu, H. F., & Le Breton, N. (2010). Structural development of the lower Paleozoic belt of South China: Genesis of an intracontinental orogen. *Journal of Asian Earth Sciences*, *39*(4), 309–330. https://doi.org/10.1016/j.jseaes.2010.03.006

Charvet, J., Shu, L. S., Shi, Y. S., Guo, L. Z., & Faure, M. (1996). The building of South China: Collision of Yangzi and Cathaysia blocks, problems and tentative answers. *Journal of Southeast Asian Earth Sciences*, *13*(3-5), 223–235. https://doi.org/10.1016/0743-9547(96)00029-3

Chu, Y., Faure, M., Lin, W., & Wang, Q. C. (2012). Early Mesozoic tectonics of the South China block: Insights from the Xuefengshan intracontinental orogen. *Journal of Asian Earth Sciences*, *61*, 199–220. https://doi.org/10.1016/j.jseaes.2012.09.029

Chu, Y., Faure, M., Lin, W., Wang, Q. C., & Ji, W. B. (2012). Tectonics of the Middle Triassic intracontinental Xuefengshan belt, South China: New insights from structural and chronological constraints on the basal décollement zone. *International Journal of Earth Sciences*, *101*(8), 2125–2150. https://doi.org/10.1007/s00531-012-0780-5

Chu, Y., & Lin, W. (2014). Phanerozoic polyorogenic deformation in southern Jiuling massif, northern South China Block: Constraints from structural analysis and geochronology. *Journal of Asian Earth Sciences*, *86*, 117–130. https://doi.org/10.1016/j.jseaes.2013.05.019

Chu, Y., Lin, W., Faure, M., Wang, Q. C., & Ji, W. B. (2012). Phanerozoic tectonothermal events of the Xuefengshan belt, central South China: Implications from U–Pb age and Lu–Hf determinations of granites. *Lithos*, *150*, 243–255. https://doi.org/10.1016/j.lithos.2012.04.005

Cocherie, A., & Albarède, F. (2001). An improved U–Th–Pb age calculation for electron microprobe dating of monazite. *Geochimica et Cosmochimica Acta*, *65*(24), 4509–4522. https://doi.org/10.1016/S0016-7037(01)00753-0

Cocherie, A., Legendre, O., Peucat, J. J., & Kouamelan, A. N. (1998). Geochronology of polygenetic monazites constrained by in situ electron microprobe Th–U–total lead determination: Implications for lead behaviour in monazite. *Geochimica et Cosmochimica Acta*, *62*(14), 2475–2497. https://doi.org/10.1016/S0016-7037(98)00171-9

Davis, G. A., & Darby, B. J. (2010). Early Cretaceous overprinting of the Mesozoic Daqing Shan fold-and-thrust belt by the Hohhot metamorphic core complex, Inner Mongolia, China. *Geoscience Frontiers*, *1*(1), 1–20. https://doi.org/10.1016/j.gsf.2010.08.001

Davis, G. A., Darby, B. J., Zheng, Y. D., & Spell, T. L. (2002). Geometric and temporal evolution of an extensional detachment fault, Hohhot metamorphic core complex, Inner Mongolia, China. *Geology*, *30*(11), 1003–1006. https://doi.org/10.1130/0091-7613(2002)030%3C1003:GATEOA%3E2.0.CO;2

Dodson, M. H. (1973). Closure temperature in cooling geochronological and petrological systems. *Contributions to Mineralogy and Petrology*, *40*(3), 259–274. https://doi.org/10.1007/BF00373790

Dong, S. W., Zhang, Y. Q., Zhang, F. Q., Cui, J. J., Chen, X. H., Zhang, S. H., … Li, H. L. (2015). Late Jurassic–Early Cretaceous continental convergence and intracontinental orogenesis in East Asia: A synthesis of the Yanshan revolution. *Journal of Asian Earth Sciences*, *114*, 750–770. https://doi.org/10.1016/j.jseaes.2015.08.011

Dong, Y. P., Zhang, G. W., Neubauer, F., Liu, X. M., Genser, J., & Hauzenberger, C. (2011). Tectonic evolution of the Qinling orogen, China: Review and synthesis. *Journal of Asian Earth Sciences*, *41*(3), 213–237. https://doi.org/10.1016/j.jseaes.2011.03.002

Faure, M., Lepvrier, C., Nguyen, V. V., Vu, V. T., Lin, W., & Chen, Z. C. (2014). The South China Block–Indochina collision: Where, when, and how? *Journal of Asian Earth Sciences*, *79*, 260–274. https://doi.org/10.1016/j.jseaes.2013.09.022

Faure, M., Lin, W., Chu, Y., & Lepvrier, C. (2016). Triassic tectonics of the southern margin of the South China Block. *Comptes Rendus Geoscience*, *348*(1), 5–14. https://doi.org/10.1016/j.crte.2015.06.012

Faure, M., Shu, L. S., Wang, B., Charvet, J., Choulet, F., & Monié, P. (2009). Intracontinental subduction: A possible mechanism for the Early Palaeozoic orogen of SE China. *Terra Nova*, *21*(5), 360–368. https://doi.org/10.1111/j.1365-3121.2009.00888.x

Faure, M., Sun, Y., Shu, L. S., Monié, P., & Charvet, J. (1996). Extensional tectonics within a subduction-type orogen. The case study of the Wugongshan dome (Jiangxi Province, southeastern China). *Tectonophysics*, *263*(1-4), 77–106. https://doi.org/10.1016/S0040-1951(97)81487-4

Gao, L. Z., Chen, J., Ding, X. Z., Liu, Y. R., Zhang, C. H., Zhang, H., … Zhang, Y. H. (2011). Zircon SHRIMP U–Pb dating of the tuff bed of Lengjiaxi and Banxi groups, northeastern Hunan: Constraints on the Wuling movement [in Chinese with English abstract]. *Geological Bulletin of China*, *30*, 1001–1008.

Gao, S., Yang, J., Zhou, L., Li, M., Hu, Z. C., Guo, J. L., … Wei, J. Q. (2011). Age and growth of the Archean Kongling terrain, South China, with emphasis on 3.3 Ga granitoid gneisses. *American Journal of Science*, *311*(2), 153–182. https://doi.org/10.2475/02.2011.03

Gilder, S. A., Gill, J., Coe, R. S., Zhao, X. X., Liu, Z. W., Wang, G. X., … Wu, H. R. (1996). Isotopic and paleomagnetic constraints on the Mesozoic tectonic evolution of south China. *Journal of Geophysical Research*, *101*(B7), 16,137–16,154. https://doi.org/10.1029/96JB00662

Gilder, S. A., Keller, G. R., Luo, M., & Goodell, P. C. (1991). Timing and spatial distribution of rifting in China. *Tectonophysics*, *197*(2-4), 225–243. https://doi.org/10.1016/0040-1951(91)90043-R

Gu, X. X., Liu, J. M., Zheng, M. H., Tang, J. X., & Qi, L. (2002). Provenance and tectonic setting of the Proterozoic turbidites in Hunan, South China: Geochemical evidence. *Journal of Sedimentary Research*, *72*(3), 393–407. https://doi.org/10.1306/081601720393

Hu, J. M., Chen, H., Qu, H. J., Wu, G. L., Yang, J. X., & Zhang, Z. Y. (2012). Mesozoic deformations of the Dabashan in the southern Qinling orogen, central China. *Journal of Asian Earth Sciences*, *47*, 171–184. https://doi.org/10.1016/j.jseaes.2011.12.015

Ji, W. B., Chen, Y., Chen, K., Wei, W., Faure, M., & Lin, W. (2017). Multiple emplacement and exhumation history of the Late Mesozoic Dayunshan–Mufushan batholith in southeast China and its tectonic significance: 2. Magnetic fabrics and gravity survey. *Journal of Geophysical Research: Solid Earth*, *122*. https://doi.org/10.1002/2017JB014598

Ji, W. B., Lin, W., Faure, M., Chen, Y., Chu, Y., & Xue, Z. H. (2017). Origin of the Late Jurassic to Early Cretaceous peraluminous granitoids in the northeastern Hunan province (middle Yangtze region), South China: Geodynamic implications for the paleo-Pacific subduction. *Journal of Asian Earth Sciences*, *141*, 174–193. https://doi.org/10.1016/j.jseaes.2016.07.005

Ji, W. B., Lin, W., Faure, M., Chu, Y., Wu, L., Wang, F., … Wang, Q. C. (2014). Origin and tectonic significance of the Huangling massif within the Yangtze craton, South China. *Journal of Asian Earth Sciences*, *86*, 59–75. https://doi.org/10.1016/j.jseaes.2013.06.007

Ji, W. B., Lin, W., Faure, M., Shi, Y. H., & Wang, Q. C. (2017). The Early Cretaceous orogen-scale Dabieshan metamorphic core complex: Implications for extensional collapse of the Triassic HP–UHP orogenic belt in east-central China. *International Journal of Earth Sciences*, *106*(4), 1311–1340. https://doi.org/10.1007/s00531-016-1311-6

Jiang, Y. H., Jiang, S. Y., Dai, B. Z., Liao, S. Y., Zhao, K. D., & Ling, H. F. (2009). Middle to late Jurassic felsic and mafic magmatism in southern Hunan province, southeast China: Implications for a continental arc to rifting. *Lithos*, *107*(3-4), 185–204. https://doi.org/10.1016/j.lithos.2008.10.006

Jiang, Y. H., Zhao, P., Zhou, Q., Liao, S. Y., & Jin, G. D. (2011). Petrogenesis and tectonic implications of Early Cretaceous S- and A-type granites in the northwest of the Gan-Hang rift, SE China. *Lithos*, *121*(1-4), 55–73. https://doi.org/10.1016/j.lithos.2010.10.001

Koppers, A. A. P. (2002). ArArCALC—Software for $^{40}Ar/^{39}Ar$ age calculations. *Computational Geosciences*, *28*(5), 605–619. https://doi.org/10.1016/S0098-3004(01)00095-4

Li, J. H., Shi, W., Zhang, Y. Q., Dong, S. W., & Ma, Z. L. (2016). Thermal evolution of the Hengshan extensional dome in central South China and its tectonic implications: New insights into low-angle detachment formation. *Gondwana Research*, *35*, 425–441. https://doi.org/10.1016/j.gr.2015.06.008

Li, J. H., Zhang, Y. Q., Dong, S. W., & Johnston, S. T. (2014). Cretaceous tectonic evolution of South China: A preliminary synthesis. *Earth Science Reviews*, *134*, 98–136. https://doi.org/10.1016/j.earscirev.2014.03.008

Li, J. H., Zhang, Y. Q., Dong, S. W., & Shi, W. (2013). Structural and geochronological constraints on the Mesozoic tectonic evolution of the north Dabashan zone, south Qinling, central China. *Journal of Asian Earth Sciences*, *64*, 99–114. https://doi.org/10.1016/j.jseaes.2012.12.001

Li, J. H., Zhang, Y. Q., Dong, S. W., Su, J. B., Li, Y., Cui, J. J., & Shi, W. (2013). The Hengshan low-angle normal fault zone: Structural and geochronological constraints on the Late Mesozoic crustal extension in South China. *Tectonophysics*, *606*, 97–115. https://doi.org/10.1016/j.tecto.2013.05.013

Li, S. Z., Santosh, M., Zhao, G. C., Zhang, G. W., & Jin, C. (2012). Intracontinental deformation in a frontier of super-convergence: A perspective on the tectonic milieu of the South China Block. *Journal of Asian Earth Sciences*, *49*, 313–329. https://doi.org/10.1016/j.jseaes.2011.07.026

Li, X. F., & Yu, Y. (1991). Lead-zinc mineralization associated with Mufu Mountains metamorphic core complex and denudational faulting in the Taolin area, Hunan province, China [in Chinese with English abstract]. *Geotectonica et Metallogenia*, *15*, 90–99.

Li, X. H. (2000). Cretaceous magmatism and lithospheric extension in southeast China. *Journal of Asian Earth Sciences*, *18*(3), 293–305. https://doi.org/10.1016/S1367-9120(99)00060-7

Li, X. H., Li, W. X., Li, Z. X., Lo, C. H., Wang, J., Ye, M. F., & Yang, Y. H. (2009). Amalgamation between the Yangtze and Cathaysia blocks in South China: Constraints from SHRIMP U–Pb zircon ages, geochemistry and Nd–Hf isotopes of the Shuangxiwu volcanic rocks. *Precambrian Research*, *174*(1-2), 117–128. https://doi.org/10.1016/j.precamres.2009.07.004

Li, X. H., Li, Z. X., Ge, W. C., Zhou, H. W., Li, W. X., Liu, Y., & Wingate, M. T. D. (2003). Neoproterozoic granitoids in South China: Crustal melting above a mantle plume at *ca*. 825 Ma? *Precambrian Research*, *122*(1-4), 45–83. https://doi.org/10.1016/S0301-9268(02)00207-3

Li, X. H., Li, Z. X., & Li, W. X. (2014). Detrital zircon U–Pb age and Hf isotope constrains on the generation and reworking of Precambrian continental crust in the Cathaysia Block, South China: A synthesis. *Gondwana Research*, *25*(3), 1202–1215. https://doi.org/10.1016/j.gr.2014.01.003

Li, Z. X., Li, X. H., Wartho, J. A., Clark, C., Li, W. X., Zhang, C. L., & Bao, C. M. (2010). Magmatic and metamorphic events during the early Paleozoic Wuyi–Yunkai orogeny, southeastern South China: New age constraints and pressure–temperature conditions. *Geological Society of America Bulletin*, *122*(5-6), 772–793. https://doi.org/10.1130/B30021.1

Lin, W., Charles, N., Chen, K., Chen, Y., Faure, M., Wu, L., … Wang, Q. C. (2013). Late Mesozoic compressional to extensional tectonics in the Yiwulüshan massif, NE China and its bearing on the evolution of the Yinshan–Yanshan orogenic belt part II: Anisotropy of magnetic susceptibility and gravity modeling. *Gondwana Research*, *23*(1), 78–94. https://doi.org/10.1016/j.gr.2012.02.012

Lin, W., Faure, M., Chen, Y., Ji, W. B., Wang, F., Wu, L., … Wang, Q. C. (2013). Late Mesozoic compressional to extensional tectonics in the Yiwulüshan massif, NE China and its bearing on the evolution of the Yinshan–Yanshan orogenic belt part I: Structural analyses and geochronological constraints. *Gondwana Research*, *23*(1), 54–77. https://doi.org/10.1016/j.gr.2012.02.013

Lin, W., Faure, M., Monié, P., Schärer, U., & Panis, D. (2008). Mesozoic extensional tectonics in eastern Asia: The South Liaodong Peninsula metamorphic core complex (NE China). *Journal of Geology*, *116*(2), 134–154. https://doi.org/10.1086/527456

Lin, W., Faure, M., Monié, P., Schärer, U., Zhang, L. S., & Sun, Y. (2000). Tectonics of SE China: New insights from the Lushan massif (Jiangxi Province). *Tectonics*, *19*(5), 852–871. https://doi.org/10.1029/2000TC900009

Lin, W., Ji, W. B., Faure, M., Wu, L., Li, Q. L., Shi, Y. H., … Wang, Q. C. (2015). Early Cretaceous extensional reworking of the Triassic HP–UHP metamorphic orogen in eastern China. *Tectonophysics*, *662*, 256–270. https://doi.org/10.1016/j.tecto.2015.05.028

Lin, W., Monié, P., Faure, M., Schärer, U., Shi, Y. H., Le Breton, N., & Wang, Q. C. (2011). Cooling paths of the NE China crust during the Mesozoic extensional tectonics: Example from the south-Liaodong peninsula metamorphic core complex. *Journal of Asian Earth Sciences*, *42*(5), 1048–1065. https://doi.org/10.1016/j.jseaes.2010.09.007

Lin, W., & Wang, Q. C. (2006). Late Mesozoic extensional tectonics in North China Block: A crustal response to subcontinental mantle removal? *Bulletin de la Société Géologique de France*, *177*(6), 287–297. https://doi.org/10.2113/gssgfbull.177.6.287

Lin, W., Wang, Q. C., & Chen, K. (2008). Phanerozoic tectonics of South China Block: New insights from the polyphase deformation in the Yunkai massif. *Tectonics*, *27*, TC6004. https://doi.org/10.1029/2007TC002207

Liu, J. L., Gregory, A. D., Lin, Z. Y., & Wu, F. Y. (2005). The Liaonan metamorphic core complex, southeastern Liaoning Province, North China: A likely contributor to Cretaceous rotation of eastern Liaoning, Korea and contiguous areas. *Tectonophysics*, *407*(1-2), 65–80. https://doi.org/10.1016/j.tecto.2005.07.001

Liu, J. L., Shen, L., Ji, M., Guan, H. M., Zhang, Z. C., & Zhao, Z. D. (2013). The Liaonan/Wanfu metamorphic core complexes in the Liaodong Peninsula: Two stages of exhumation and constraints on the destruction of the North China craton. *Tectonics*, *32*(5), 1121–1141. https://doi.org/10.1002/tect.20064

Liu, S. F., Li, W. P., Wang, K., Qian, T., & Jiang, C. X. (2015). Late Mesozoic development of the southern Qinling–Dabieshan foreland fold-thrust belt, Central China, and its role in continent–continent collision. *Tectonophysics*, *644–645*, 220–234.

Ludwig, K. R. (2003). User's manual for Isoplot 3.00: A geochronological toolkit for Microsoft Excel, Berkeley Geochronology Center Special Publication No. 4.

McDougall, I., & Harrison, T. M. (1999). *Geochronology and thermochronology by the $^{40}Ar/^{39}Ar$ Method*, (second ed.). Oxford, UK: Oxford University Press.

Meng, Q. R. (2003). What drove late Mesozoic extension of the northern China–Mongolia tract? *Tectonophysics*, *369*(3-4), 155–174. https://doi.org/10.1016/S0040-1951(03)00195-1

Meng, Q. R., Wang, E., & Hu, J. M. (2005). Mesozoic sedimentary evolution of the northwest Sichuan basin: Implication for continued clockwise rotation of the South China Block. *Geological Society of America Bulletin*, *117*(3), 396–410. https://doi.org/10.1130/B25407.1

Meng, Q. X., Zhang, J., Geng, J. Z., Zhang, C. L., & Huang, W. C. (2013). Zircon U–Pb age and Hf isotope compositions of Lengjiaxi and Banxi groups in middle Hunan province: Implication for Neoproterozoic tectonic evolution in South China [in Chinese with English abstract]. *Geology in China*, *40*, 191–216.

Menzies, M., Xu, Y. G., Zhang, H. F., & Fan, W. M. (2007). Integration of geology, geophysics and geochemistry: A key to understanding the North China craton. *Lithos*, *96*(1-2), 1–21. https://doi.org/10.1016/j.lithos.2006.09.008

Parrish, R. R. (1990). U–Pb dating of monazite and its application to geological problems. *Canadian Journal of Earth Sciences*, *27*(11), 1431–1450. https://doi.org/10.1139/e90-152

Passchier, C. W., & Trouw, R. A. J. (2005). *Microtectonics* (2nd ed.). Berlin: Springer.

Paterson, S. R., Vernon, R. H., & Tobisch, O. T. (1989). A review of criteria for the identification of magmatic and tectonic foliations in granitoids. *Journal of Structural Geology*, *11*(3), 349–363. https://doi.org/10.1016/0191-8141(89)90074-6

Pommier, A., Cocherie, A., & Legendre, O. (2002). EPMA dating user's manual: Age calculation from electron probe microanalyser measurements of U–Th–Pb, Bureau de Recherches Géologiques et Minières (internal report).

Qiu, Y. M., Gao, S., McNaughton, N. J., Groves, D. I., & Ling, W. L. (2000). First evidence of $>$ 3.2 Ga continental crust in the Yangtze craton of south China and its implications for Archean crustal evolution and Phanerozoic tectonics. *Geology*, *28*(1), 11–14. https://doi.org/10.1130/0091-7613(2000)028%3C0011:FEOGCC%3E2.0.CO;2

Shen, C. B., Mei, L. F., Min, K., Jonckheere, R., Ratschbacher, L., Yang, Z., … Liu, Z. Q. (2012). Multi-chronometric dating of the Huarong granitoids from the middle Yangtze craton: Implications for the tectonic evolution of eastern China. *Journal of Asian Earth Sciences*, *52*, 73–87. https://doi.org/10.1016/j.jseaes.2012.02.013

Shen, X. M., Zhang, H. X., & Zhang, B. Y. (2008). A preliminary study of relationship between metamorphic core complexes and lithospheric thinning over the Mesozoic in South China [in Chinese with English abstract]. *Geotectonica et Metallogenia*, *32*, 11–19.

Shi, H. C., Shi, X. B., Yang, X. Q., & Jiang, H. Y. (2013). The exhumation process of Mufushan granite in Jiangnan uplift since Cenozoic: Evidence from low-temperature thermochronology. *Chinese Journal of Geophysics*, *56*, 273–286.

Shi, W., Zhang, Y. Q., Dong, S. W., Hu, J. M., Wiesinger, M., Ratschbacher, L., … Li, H. L. (2012). Intra-continental Dabashan orocline, southwestern Qinling, central China. *Journal of Asian Earth Sciences*, *46*, 20–38. https://doi.org/10.1016/j.jseaes.2011.10.005

Shu, L. S., Jahn, B. M., Charvet, J., Santosh, M., Wang, B., Xu, X. S., & Jiang, S. Y. (2014). Intraplate tectono-magmatism in the Cathaysia Block (South China): Evidence from stratigraphic, structural, geochemical and geochronological investigations. *American Journal of Science*, *314*(1), 154–186. https://doi.org/10.2475/01.2014.05

Shu, L. S., Zhou, X. M., Deng, P., Wang, B., Jiang, S. Y., Yu, J. H., & Zhao, X. X. (2009). Mesozoic tectonic evolution of the Southeast China Block: New insights from basin analysis. *Journal of Asian Earth Sciences*, *34*(3), 376–391. https://doi.org/10.1016/j.jseaes.2008.06.004

Vernon, R. H. (2000). Review of microstructural evidence of magmatic and solid-state flow. *Electronic Geosciences*, *5*, 2.

Wang, D. Z., & Shu, L. S. (2012). Late Mesozoic basin and range tectonics and related magmatism in Southeast China. *Geoscience Frontiers*, *3*(2), 109–124. https://doi.org/10.1016/j.gsf.2011.11.007

Wang, E., Meng, Q. R., Burchfiel, B. C., & Zhang, G. W. (2003). Mesozoic large-scale lateral extrusion and uplift of the Tongbai–Dabie Shan belt in east China. *Geology*, *31*(4), 307–310. https://doi.org/10.1130/0091-7613(2003)031%3C0307:MLSLER%3E2.0.CO;2

Wang, F., He, H. Y., Zhu, R. X., Sang, H. Q., Wang, Y. L., & Yang, L. K. (2006). Intercalibration of international and domestic $^{40}Ar/^{39}Ar$ dating standards. *Science in China Series D: Earth Sciences*, *49*(5), 461–470. https://doi.org/10.1007/s11430-006-0461-y

Wang, F., Wang, Q. C., Lin, W., Wu, L., Shi, W. B., Feng, H. L., & Zhu, R. X. (2014). $^{40}Ar/^{39}Ar$ geochronology of the North China and Yangtze cratons: New constraints on Mesozoic cooling and cratonic destruction under East Asia. *Journal of Geophysical Research: Solid Earth*, *119*, 3700–3721. https://doi.o10.1002/2013JB010708

Wang, J., & Li, Z. X. (2003). History of Neoproterozoic rift basins in South China: Implications for Rodinia break-up. *Precambrian Research*, *122*(1-4), 141–158. https://doi.org/10.1016/S0301-9268(02)00209-7

Wang, J. Q., Shu, L. S., Santosh, M., & Xu, Z. Q. (2015). The pre-Mesozoic crustal evolution of the Cathaysia Block, South China: Insights from geological investigation, zircon U–Pb geochronology, Hf isotope and REE geochemistry from the Wugongshan complex. *Gondwana Research*, *28*(1), 225–245. https://doi.org/10.1016/j.gr.2014.03.008

Wang, L. X., Ma, C. Q., Zhang, C., Zhang, J. Y., & Marks, M. A. W. (2014). Genesis of leucogranite by prolonged fractional crystallization: A case study of the Mufushan complex, South China. *Lithos*, *206–207*, 147–163.

Wang, T., Guo, L., Zheng, Y. D., Donskaya, T., Gladkochub, D., Zeng, L. S., … Mazukabzov, A. (2012). Timing and processes of late Mesozoic mid-lower-crustal extension in continental NE Asia and implications for the tectonic setting of the destruction of the North China craton: Mainly constrained by zircon U–Pb ages from metamorphic core complexes. *Lithos*, *154*, 315–345. https://doi.org/10.1016/j.lithos.2012.07.020

Wang, T., Zheng, Y. D., Zhang, J. J., Zeng, L. S., Donskaya, T., Guo, L., & Li, J. B. (2011). Pattern and kinematic polarity of late Mesozoic extension in continental NE Asia: Perspectives from metamorphic core complexes. *Tectonics*, *30*, TC6007. https://doi.org/10.1029/2011TC002896

Wang, W., Zhou, M. F., Yan, D. P., Li, L., & Malpas, J. (2013). Detrital zircon record of Neoproterozoic active-margin sedimentation in the eastern Jiangnan Orogen, South China. *Precambrian Research*, *235*, 1–19. https://doi.org/10.1016/j.precamres.2013.05.013

Wang, X. L., Zhou, J. C., Griffin, W. L., Zhao, G. C., Yu, J. H., Qiu, J. S., … Xing, G. F. (2014). Geochemical zonation across a Neoproterozoic orogenic belt: Isotopic evidence from granitoids and metasedimentary rocks of the Jiangnan orogen, China. *Precambrian Research*, *242*, 154–171. https://doi.org/10.1016/j.precamres.2013.12.023

Wang, X. L., Zhou, J. C., Wan, Y. S., Kitajima, K., Wang, D., Bonamici, C., … Sun, T. (2013). Magmatic evolution and crustal recycling for Neoproterozoic strongly peraluminous granitoids from southern China: Hf and O isotopes in zircon. *Earth and Planetary Science Letters*, *366*, 71–82. https://doi.org/10.1016/j.epsl.2013.02.011

Wang, Y. J., Fan, W. M., Zhang, G. W., & Zhang, Y. H. (2013). Phanerozoic tectonics of the South China Block: Key observations and controversies. *Gondwana Research*, *23*(4), 1273–1305. https://doi.org/10.1016/j.gr.2012.02.019

Wei, W., Chen, Y., Faure, M., Martelet, G., Lin, W., Wang, Q. C., … Hou, Q. L. (2016). An early extensional event of the South China Block during the Late Mesozoic recorded by the emplacement of the Late Jurassic syntectonic Hengshan composite granitic massif (Hunan, SE China). *Tectonophysics*, *672–673*, 50–67.

Wei, W., Chen, Y., Faure, M., Shi, Y. H., Martelet, G., Hou, Q. L., … Wang, Q. C. (2014). A multidisciplinary study on the emplacement mechanism of the Qingyang–Jiuhua massif in southeast China and its tectonic bearings. Part I: Structural geology, AMS and paleomagnetism. *Journal of Asian Earth Sciences*, *86*, 76–93. https://doi.org/10.1016/j.jseaes.2013.06.003

Wei, W., Faure, M., Chen, Y., Ji, W. B., Lin, W., Wang, Q. C., … Hou, Q. L. (2015). Back-thrusting response of continental collision: Early Cretaceous NW-directed thrusting in the Changle–Nan'ao belt (Southeast China). *Journal of Asian Earth Sciences*, *100*, 98–114. https://doi.org/10.1016/j.jseaes.2015.01.005

Wei, W., Martelet, G., Le Breton, N., Shi, Y. H., Faure, M., Chen, Y., … Wang, Q. C. (2014). A multidisciplinary study of the emplacement mechanism of the Qingyang–Jiuhua massif in Southeast China and its tectonic bearings. Part II: Amphibole geobarometry and gravity modeling. *Journal of Asian Earth Sciences*, *86*, 94–105. https://doi.org/10.1016/j.jseaes.2013.09.021

Wong, J., Sun, M., Xing, G. F., Li, X. H., Zhao, G. C., Wong, K., … Wu, F. Y. (2009). Geochemical and zircon U–Pb and Hf isotopic study of the Baijuhuajian metaluminous A-type granite: Extension at 125–100 Ma and its tectonic significance for South China. *Lithos*, *112*(3-4), 289–305. https://doi.org/10.1016/j.lithos.2009.03.009

Wu, F. Y., Ji, W. Q., Sun, D. H., Yang, Y. H., & Li, X. H. (2012). Zircon U–Pb geochronology and Hf isotopic compositions of the Mesozoic granites in southern Anhui Province, China. *Lithos*, *150*, 6–25. https://doi.org/10.1016/j.lithos.2012.03.020

Wu, F. Y., Xu, Y. G., Gao, S., & Zheng, J. P. (2008). Lithospheric thinning and destruction of the North China craton [in Chinese with English abstract]. *Acta Petrologica Sinica*, *2008*(24), 1145–1174.

Wu, Y. B., & Zheng, Y. F. (2013). Tectonic evolution of a composite collision orogen: An overview on the Qinling–Tongbai–Hong'an–Dabie–Sulu orogenic belt in central China. *Gondwana Research*, *23*(4), 1402–1428. https://doi.org/10.1016/j.gr.2012.09.007

Xu, D. R., Gu, X. X., Li, P. C., Chen, G. H., Xia, B., Bachlinski, R., … Fu, G. G. (2007). Mesoproterozoic–Neoproterozoic transition: Geochemistry, provenance and tectonic setting of clastic sedimentary rocks on the SE margin of the Yangtze Block, South China. *Journal of Asian Earth Sciences*, *29*, 637–650.

Yan, C. L., Shu, L. S., Santosh, M., Yao, J. L., Li, J. Y., & Li, C. (2015). The Precambrian tectonic evolution of the western Jiangnan Orogen and western Cathaysia Block: Evidence from detrital zircon age spectra and geochemistry of clastic rocks. *Precambrian Research*, *268*, 33–60. https://doi.org/10.1016/j.precamres.2015.07.002

Yan, D. P., Zhang, B., Zhou, M. F., Wei, G. Q., Song, H. L., & Liu, S. F. (2009). Constraints on the depth, geometry and kinematics of blind detachment faults provided by fault propagation folds: An example from the Mesozoic fold belt of South China. *Journal of Structural Geology*, *31*(2), 150–162. https://doi.org/10.1016/j.jsg.2008.11.005

Yan, D. P., Zhou, M. F., Song, H. L., Wang, X. W., & Malpas, J. (2003). Origin and tectonic significance of a Mesozoic multi-layer over-thrust system within the Yangtze Block (South China). *Tectonophysics*, *361*(3-4), 239–254. https://doi.org/10.1016/S0040-1951(02)00646-7

Yang, S. Y., Jiang, S. Y., Zhao, K. D., Jiang, Y. H., Ling, H. F., & Luo, L. (2012). Geochronology, geochemistry and tectonic significance of two Early Cretaceous A-type granites in the Gan-Hang Belt, southeast China. *Lithos*, *150*, 155–170. https://doi.org/10.1016/j.lithos.2012.01.028

Yu, A. N., Ye, B. L., & Peng, E. S. (1998). Relationship between the Dayunshan metamorphic core complex and mineralization, Taolin, Hunan province [in Chinese with English abstract]. *Geotectonica et Metallogenia*, *22*, 82–88.

Yu, J. H., O'Reilly, S. Y., Wang, L. J., Griffin, W. L., Zhou, M. F., Zhang, M., & Shu, L. S. (2010). Components and episodic growth of Precambrian crust in the Cathaysia Block, South China: Evidence from U–Pb ages and Hf isotopes of zircons in Neoproterozoic sediments. *Precambrian Research*, *181*(1-4), 97–114. https://doi.org/10.1016/j.precamres.2010.05.016

Zhao, G. C. (2015). The Jiangnan Orogen in South China: Developing from divergent double subduction. *Gondwana Research*, *27*(3), 1173–1180. https://doi.org/10.1016/j.gr.2014.09.004

Zhao, J. H., Zhou, M. F., Yan, D. P., Zheng, J. P., & Li, J. W. (2011). Reappraisal of the ages of Neoproterozoic strata in South China: No connection with the Grenvillian orogeny. *Geology*, *39*(4), 299–302. https://doi.org/10.1130/G31701.1

Zhao, J. H., Zhou, M. F., & Zheng, J. P. (2013). Constraints from zircon U–Pb ages, O and Hf isotopic compositions on the origin of Neoproterozoic peraluminous granitoids from the Jiangnan fold belt, South China. *Contributions to Mineralogy and Petrology*, *166*(5), 1505–1519. https://doi.org/10.1007/s00410-013-0940-z

Zhou, X. M., & Li, W. X. (2000). Origin of Late Mesozoic igneous rocks in southeastern China: Implications for lithosphere subduction and underplating of mafic magmas. *Tectonophysics*, *326*(3-4), 269–287. https://doi.org/10.1016/S0040-1951(00)00120-7

Zhou, X. M., Sun, T., Shen, W. Z., Shu, L. S., & Niu, Y. L. (2006). Petrogenesis of Mesozoic granitoids and volcanic rocks in South China: A response to tectonic evolution. *Episodes*, *29*, 26–33.

Zhu, G., Chen, Y., Jiang, D. Z., & Lin, S. Z. (2015). Rapid change from compression to extension in the North China craton during the Early Cretaceous: Evidence from the Yunmengshan metamorphic core complex. *Tectonophysics*, *65*, 691–110.

Zhu, G., Jiang, D. Z., Zhang, B. L., & Chen, Y. (2012). Destruction of the eastern North China craton in a backarc setting: Evidence from crustal deformation kinematics. *Gondwana Research*, *22*(1), 86–103. https://doi.org/10.1016/j.gr.2011.08.005

Zhu, G., Xie, C. L., Chen, W., Xiang, B. W., & Hu, Z. Q. (2010). Evolution of the Hongzhen metamorphic core complex: Evidence for Early Cretaceous extension in the eastern Yangtze craton, eastern China. *Geological Society of America Bulletin*, *122*(3-4), 506–516. https://doi.org/10.1130/B30028.1

Zhu, Q. B., Yang, K. G., & Wang, Y. (2010). Extensional detachment and magmatism of the Lushan metamorphic core complex: Constraints from $^{40}Ar/^{39}Ar$ and U–Pb geochronology [in Chinese with English abstract]. *Geotectonica et Metallogenia*, *34*, 391–401.

Zhu, R. X., Xu, Y. G., Zhu, G., Zhang, H. F., Xia, Q. K., & Zheng, T. Y. (2012). Destruction of the North China craton. *Science China Earth Sciences*, *55*(10), 1565–1587. https://doi.org/10.1007/s11430-012-4516-y